Geotech Geol Eng (2024) 42:207–234
https://doi.org/10.1007/s10706-023-02565-8

ORIGINAL PAPER

Investigating the Influence of Geometric Factors on Tunnel Stability: A Study on Arched Roofs

Wael R. Abdellah · Stephen D. Butt · Ahmed I. Abdullah · Ahmed Rushdy Towfeek · Mahrous A. M. Ali

Received: 25 May 2023 / Accepted: 8 July 2023 / Published online: 9 August 2023

Abstract This research investigates the influence of rock joint dip angle and spacing on the performance of arched roof tunnels. A sensitivity analysis was conducted using Rocscience RS2 software, enabling the evaluation of stress distribution and rock mass deformation. The analysis involved the identification of specific reference points on the tunnel's back, walls, and floor to assess stress state, deformation, and the extent of plastic damage zones near the tunnel's perimeter, in relation to the minimum embedment length of the primary rock support. The results revealed distinct stress patterns within the tunnel system. Tensile-induced stresses were minimal along the tunnel walls, while high compressive-induced stresses were observed around the tunnel's back/roof and floor. Additionally, substantial rock deformation was observed at the tunnel's periphery, as evidenced by measurements taken at the reference points. Notably, an increase in the dip angle of the joints resulted in reduced displacement, suggesting a potential strategy for mitigating deformation. Furthermore, the research highlighted the crucial role of joint spacing in ensuring tunnel stability. Decreasing joint spacing was found to impact tunnel stability significantly adversely, underscoring the importance of carefully considering joint spacing during the design and construction phases of arched roof tunnels. The analysis was validated by comparing the numerical modeling results with readings obtained from Multi-Points Borehole Extensometers (MPBXs) installed in the tunnel walls and roof. The comparison revealed variations of 16% at the tunnel's right wall, 11% at the tunnel's left wall, and 12% at the tunnel roof.

Keywords Numerical modelling · Joint dip angle · Joint spacing · Stability of arched roof tunnels

Abbreviations

WCR	Wall convergence ratio
Δ_w	Wall closure
w	The initial opening width
RSR	Roof sag ratio
Δ_S	Roof deflection
H	Initial opening vertical span
FHR	Floor heave ratio

W. R. Abdellah (✉)
Mining and Metallurgical Engineering Department, Faculty of Engineering, University of Assiut, Assiut 71516, Egypt
e-mail: waelabdellah@aun.edu.eg

S. D. Butt
Faculty of Engineering and Applied Science, Memorial University, St. John's, NL A1B 3X5, Canada

A. I. Abdullah · A. R. Towfeek
Civil Engineering Department, Faculty of Engineering-Qena, Al-Azhar University, Qena 83513, Egypt

M. A. M. Ali
Mining and Petroleum Engineering Department, Faculty of Engineering-Qena, Al-Azhar University, Qena 83511, Egypt

Δ_y	Floor lift up.
H	Initial opening vertical span
σ_1	Post-opening stress
σ^0	In-situ (Pre) stress
SF	Strength factor
UCS	Uniaxial compressive strength
SCF	Stress concentration factor

1 Introduction

Tunnels are among the most essential geotechnical structures of modern societies. They serve several functions, for example, irrigation, sanitary drainage, transportation, and power transmission; thus, it is crucial that tunnels are stable during their service life (Dong et al. 2020; Wang et al. 2019; Wu et al. 2021; Zaid 2021; Zhang and Yang 2019).

The performance of underground tunnels is strongly impacted by many elements, such as rock mass quality (Zhou and Yang 2021), the presence of discontinuities and their characteristics (e.g., dip/dip direction or orientation, spacing, length, roughness, and interconnectivity), tunnel geometry (e.g., shape and size), stress state, and depth below surface (Panji et al. 2016; Eman et al. 2013; Madkour 2012).

Many parameters strongly affect the durability of underground tunnels, such as the characteristics of the surrounding rock mass matrix (Aksoy et al. 2020; Chen et al. 2019), attributes of associated rock discontinuities (roughness, length, orientation, and interconnectivity) (Kim et al. 2020), stress environment (stress ratio, seismicity) (Lukic et al. 2020), and depth below surface (Ghorbani et al. 2015, Wasantha 2015b, Kulatilake et al. 2013, Yu et al. 2011). Joints are usually spaced and may have the same dip/dip direction, that is, they occur in parallel groups or classes; therefore, the rock mass will be divided into blocks (Jia and Tang 2008, Jaeger 1979). The stress state gains importance at greater depths. In an elevated stress environment, the resilience of underground structures is governed by the generated stresses and rock discontinuities that are concurrent or mirrored to the tunnel periphery (Abdellah et al. 2014; Martin et al. 1999). The stability of underground tunnels can be analyzed using rational, practical (e.g. experimental), or computation methods (Zhang et al. 2020). Rational or mathematical methods apply formulae to calculate the stress distribution and rock mass distortion or deformity around elementary openings (e.g., rounded, rectangular, elliptical) (Lee et al. 2020). These methods were first derived by Kirsch (1898), Brady (1977) Brady and Lorig (1988), and Ladanyi (1974). A straightforward mathematical model based on Bray's elastic solution has been proposed and presented by Chinaei et al. (2021).

Practical or graphical approaches, such as the stability graph method (Mitri et al. 2011), use historicaldataand in order to estimate the appropriate support structure, apply a rock mass classification scheme. Computation or computer-assisted techniques are effective instruments for dealing with geometries that are very complex. They can be used to evaluate tunnel stability at the prefeasibility stage of a project to decide the optimal position of the tunnel as well as after construction (Berisavljević et al. 2015, Soren and Budi 2014, Rasouli et al. 2011, Hammah et al. 2005, Potts 1999, Brinkgreve and Bakker 1991). Several studies have shown that computer-assisted method has been successfully applied to examine: the effectiveness of rock support mounted in a jointed rock mass (Li et al. 2021); the rock mass deformation around tunnels (Everling 1964; Goodman 1972); the impact of discontinuities on tunnel stability (Jeon et al. 2004); the impact of rock discontinuities on the functionality of underground openings using discontinuous deformation analysis (Yeung and Leong 1997); the effect of fault parameters on tunnel stability using two-dimensional discrete element code (Hao 2005); and the influence of rock joint dimension and orientation on tunnel stability (Jiang et al. 2006). Stress variation along the tunnel periphery based on joint dip angle and boundary conditions have been investigated by Tonon and Amadei (Tonon and Amadei 2003). A constitutive model for jointed rock masses to address the elasto-plastic behaviour of the orthotropic tunnel structure by mixing strains from joint sets and intact rock masses has been proposed by Wang and Huang (Wang and Huang 2009). Tunnel stability has also been studied using the Discrete Element Method (DEM) using block size and shape as factors (Fan et al. 2021). A uniform joint model and an inhomogeneous plastic function are used to investigate tunnel construction safety in the elasto-plastic range (Maghous et al. 2008). The objectives of this study can be summarized in the following two points:

1. Investigate the impact of variable rock joint orientation and spacing on the stability of an arched roof tunnel using a computational tool: This study aims to utilize a computational tool to analyze how different orientations and spacings of rock joints affect the stability of an arched roof tunnel. The focus is on evaluating the stress state within the tunnel, determining the depth of damaged zones surrounding the tunnel, and assessing the displacement of the disturbed rock matrix.
2. Utilize various failure assessment metrics and establish thresholds for evaluation: The paper employs multiple failure assessment metrics, including wall convergence/closure ratio, roof deflection and floor uplift ratios, induced stress, strength factor, strength concentration factor, and spread of damage zones. The study establishes specific thresholds for these evaluation measures, serving as a framework to assess the computational results and determine the stability of the tunnel under different rock joint conditions.

2 Stability Evaluation Criteria

The choice of rock failure evaluation criteria in finite element codes is influenced by several factors, including the availability of built-in functions, the specific application, the purpose of the study, and the desired level of conservativity. Available built-in functions should be assessed for their compatibility and representation of rock behavior and failure mechanisms. The application and purpose of the study guide the selection of appropriate failure criteria, considering the specific engineering context. The conservativity of results is important to strike a balance between safety and accuracy. Validation through comparisons with field observations or empirical data helps ensure the reliability of chosen criteria. Consideration of dominant failure modes, such as brittle fracture or shear failure, aids in selecting criteria that effectively capture those modes. To make an informed choice, consulting literature, experts, and code documentation is recommended. Careful assessment of these factors ensures the appropriate selection of rock failure evaluation criteria in finite element analysis.

The rock deformation criteria include the displacement or translation of the tunnel's walls, deflection ratio of the tunnel's crown or back, and up lifting ratio of the tunnel's floor. The stress state criteria include the induced stress, strength factor (i.e., resilience of rock mass relative to induced stress), and stress concentration (i.e., locations of high and low stresses) around the tunnel boundary. The yield-based criterion is used to determine the length of rock mass damaged or collapsed zones and compare them with the embedment length of primary rock support (Qiu et al. 2020).

2.1 Wall Convergence Ratio (WCR)

The WCR is the ratio of wall closure with the initial width of the tunnel as expressed in the following Equation (Zhang and Mitri 2008; Sainoki and Mitri 2014; Abdellah 2015b):

$$WCR = \left(\frac{\Delta_w}{w}\right) \times 100 \tag{1}$$

where Δ_w is the difference between the initial width, w, and the width after deformation,w_1, where $\left(\Delta_w = w - w_1\right)$. The stability of the tunnel would be considered ineffective if the WCR surpasses 1.5% (Abdellah 2015a; Wang et al. 2018; Heidarzadeh et al. 2021).

2.2 Sag ratio of the Roof/Back (RSR)

The RSR is calculated as the proportion of roof deflection, Δ_S to the initial vertical span of the opening, H, as given in the following Eq. (Zhang and Mitri 2008; Edelbro 2010):

$$\text{RSR} = \left(\frac{\Delta_S}{H}\right) \times 100 \tag{2}$$

The functioning of the tunnel would be deemed unworkable if the RSR crossed 0.5% (Abdellah 2015b; Nguyen et al. 2021; Olufe 2021).

2.3 Heave Ratio of the Floor (FHR)

The FHR is the ratio of floor lift up, Δ_y, to the vertical span of the tunnel opening, as given in the following Equation:

$$FHR = \left(\frac{\Delta_y}{H}\right) \times 100 \tag{3}$$

For the context of this research, it is presumed that the tunnel's safety is viewed inadequate if the FHR is above 0.5% (Zhang and Mitri 2008; Abdellah et al. 2018; Wasantha et al. 2021).

2.4 Induced Stress

The differential stress is the difference between the tunnel stress before and after it has been driven (Abdellah et al. 2014). If this stress goes beyond the resilience of the rock matrix surrounding the tunnel, it will collapse. The stress induced determines the difference between in-situ (virgin) stress, σ^0, and the resulting stress, σ_1, as indicated in the following Equation:

$$\text{Induced stress} = \sigma_1 - \sigma^0 \tag{4}$$

2.5 Strength Factor (SF)

The SF is the ratio of the laboratory intact rock compressive strength, UCS, to post-opening stress, σ_1, as presented in the following Equation:

$$\text{SF} = \frac{UCS}{\sigma_1} \tag{5}$$

2.6 Factor of Stress Concentration (SCF)

The SCF is the ratio of generated stress, σ_1, to the pre-mining stress, σ^0 as given in the following Equation (Zhang and Mitri 2008):

$$SCF = \frac{\sigma_1}{\sigma^0} \tag{6}$$

The magnitude of SCF indicates the location and type of stress concentration. The stability of tunnel is considered unsatisfactory if $\sigma_1 > \sigma_0$ (i.e., SCF exceeds 1.0).

2.7 Extent of Yield/Damage Zones

Damage zones, also referred to as rock failure or yielding zones. Such zones indicate specific regions within a rock mass where significant deformations, fractures, or failure mechanisms have occurred. These zones indicate areas of compromised structural integrity and reduced strength within the rock mass. They can be defined through a combination of approaches. One common method involves analyzing the behavior of the rock mass and identifying regions where significant deformations or failure mechanisms occur. This can be accomplished through field observations, monitoring data, or numerical simulations, which help identify areas exhibiting excessive displacements, deformations, or strains. Additionally, geological and geotechnical observations play a crucial role in defining damage zones. These observations consider indicators such as fracturing, joint separation, spalling, or shear zones, which provide evidence of localized failure or yielding. Rock mass rating systems, such as the Rock Mass Rating (RMR) or the Geological Strength Index (GSI), can further assist in assessing stability and identifying potential damage zones based on parameters like rock strength, joint conditions, and groundwater. Laboratory testing of rock samples collected from suspected damage zones, including uniaxial compressive strength, tensile strength, and shear strength tests, helps quantify the rock's resistance to failure and confirms the presence of damage zones. Lastly, numerical modeling techniques, such as finite element analysis or distinct element method simulations, provide insights into the behavior of the rock mass by considering its properties, joint characteristics, and loading conditions, allowing for the identification and delineation of damage zones. The integration of these approaches allows engineers and geologists to define damage zones accurately, leading to informed decisions on mitigation measures and design considerations to enhance the stability and safety of both the rock mass and any structures within it.

The yield-based function is a standard criterion for evaluation which exists in most codes of finite-elements. When a rock is compressed outside its deformable capacity, it yields. The yielding measures up the depth of plastic regions into the rock matrix around the tunnel's periphery to the least anchorage length of the installed rock support remaining in fresh/undisturbed rock mass. A rule of thumb is being used herein, whereby the shear strength of resin grouted rock rebar can sustain 1-ton of axial load per 1-inch anchorage length of the bolt (Abdellah 2014). Thus, the minimum anchorage length is estimated as 2.5 cm per ton (1 in/ton) of the rock bolt tensile strength (Abdellah et al. 2011). For a rock bolt with 12 tons of tensile capacity, the anchorage limit is 30 cm (12 in).

The stability of the tunnel is thus deemed inadequate for a 180 cm long rock bolt that is mounted, when the extent of failure zones goes beyond 150 cm. Alternatively, the bolt anchorage length left in the fresh rock mass becomes insufficient (i.e., embedment length is less than 30 cm) (Abdellah and Mitri 2016; Sinha and Chugh 2018).

3 Modelling set up

A set of models was created using RS2, a two-dimensional elastoplastic finite element commercial and research software by Rocscience Inc. (2016). RS2D employs the FEM to discretize the analysis domain into finite elements, allowing for the solution of the governing equations at discrete points. The reference tunnel is located 50 m below surface where the associated rock joints dip at an angle of 30° and the stress ratio is 2.13 (Fig. 1a). As shown in Fig. 1a, the study zone comprises of slate and limestone rock mass. The tunnel opening is driven into limestone rock mass and measures 5 m by 5 m with a gently arched back. The X- and Y-directions of the external boundary of the model are set to have zero displacement, meaning that it is fixed and cannot move or deform in these directions. This external boundary has a box-like shape, and it is expanded by a factor of ten times the size of the tunnel opening. To minimize the influence of boundaries on the numerical model results, it is crucial to ensure an adequate distance between the lateral boundary and the lower bound of the model from the top. Analysis of displacement and stress contours in the finite element software indicates that the chosen distance is indeed sufficient (Maleki and Nabizadeh 2021; Maleki and Mir Mohammad Hosseini 2022; Maleki et al. 2023).

In the numerical model shown in Fig. 1, there is an assumption of a continuous structural plane between slate and limestone, despite potential inconsistencies with the actual geological conditions. This assumption serves several purposes. Firstly, it simplifies the analysis process by making it computationally feasible, allowing for a more manageable simulation. While it may overlook the intricate geological complexities, it still provides valuable insights into the overall behavior and response of the rock mass. Secondly, the assumption can serve as an initial approximation for preliminary investigations, enabling researchers to grasp the rock mass's initial response before considering more intricate geological features. It helps evaluate the baseline behavior and explore general trends or phenomena related to rock mass stability. Thirdly, the assumption can be part of a sensitivity analysis to assess the influence of different factors on the model's results. By assuming a continuous structural plane, the study can examine the impact of other parameters, such as joint spacing, stress distribution, or material properties, on rock mass stability. This analysis provides insights into the relative importance of different factors in the overall assessment. Lastly, feasibility and resource constraints play a role in this assumption. Field investigations and obtaining detailed geological data can be challenging, time-consuming, and costly. In situations where resources or logistical constraints are limited, assumptions are made to strike a balance between available resources and study objectives, acknowledging that capturing every geological feature accurately may not be possible under such circumstances.

The tunnel primary support system uses Grade 60, 19 mm (3/4 inch) resin grouted rebars 1.8 m (6 ft) long in the walls and in the back. All nodes on the exterior perimeter are given a fixed, zero displacement boundary condition when the mesh is generated. The triangular "pin" symbols that are observed at each node of the exterior boundary show this. The gravity field stress is applied where the stress block reflects the in-plane horizontal/vertical stress ratio, which in this study is 2.13, ground surface elevation is 50 m and unit weight of overburden is 0.0255 MN/m^3. The mean values of slate and limestone rock masses are used in the model. The analysis will be set up, with the first stage consisting of tunnel excavation. Table 1 lists the two factors are being considered; joint dip angles and joint spacing: A set of models with varied joint dip angles of 0°, 15°, 30°, 45°, 60°, 75°, and 90°, joint spacing of 5 m, stress ratio of 2.13, and depth of 50 m below surface were built to explore the influence of joint orientation on tunnel stability. A set of models with joint spacing of 0.5 m, 1.5 m, 3.5 m, and 5 m, joint dip angle of 30°, stress ratio of 2.13, and depth of 50 m below surface have also been built to study the impact of joint spacing on tunnel stability. Table 2 gives the mechanical properties of the rock mass and rock joints adopted in this parametric stability analysis. These values were selected from a case study that depicts the

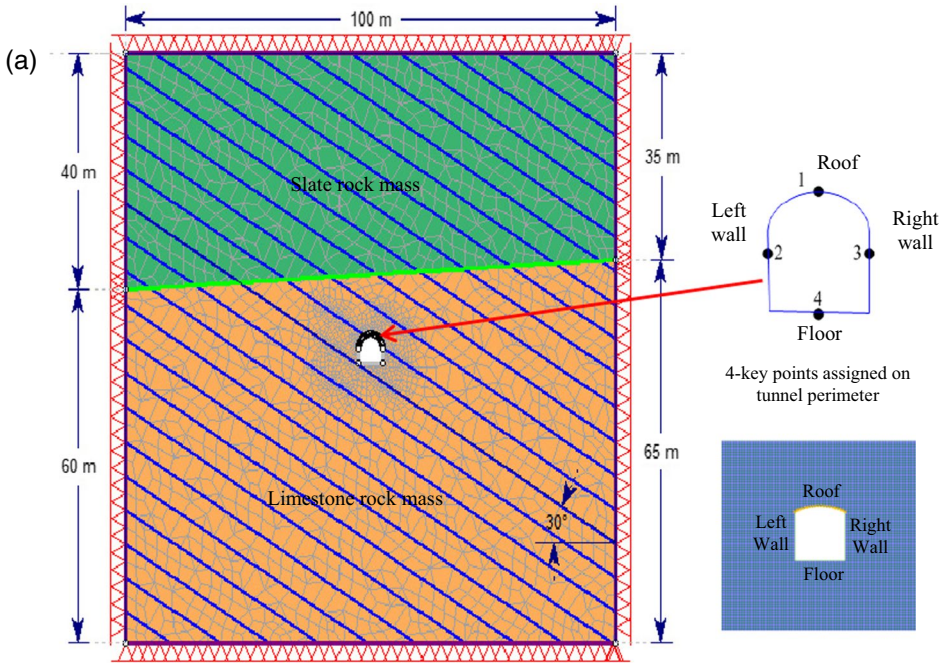
(a)
100 m
40 m
60 m
35 m
65 m
Slate rock mass
Limestone rock mass
30°
Roof
Left wall
Right wall
Floor
1
2
3
4
4-key points assigned on tunnel perimeter
Roof
Left Wall
Right Wall
Floor

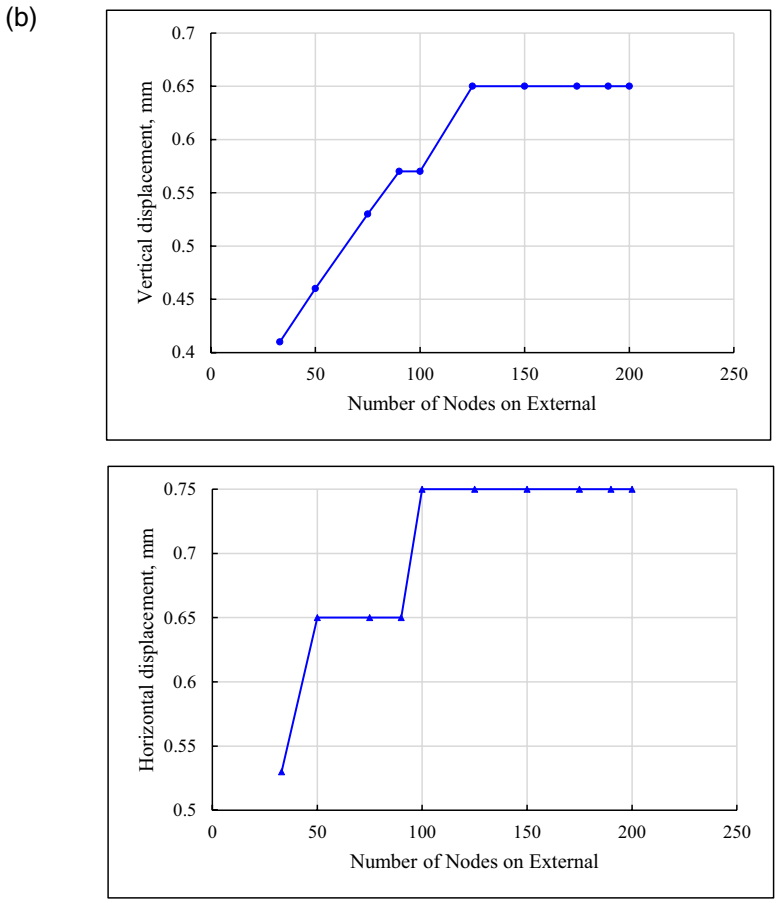
(b)
Vertical displacement, mm
0.7
0.65
0.6
0.55
0.5
0.45
0.4
0
50
100
150
200
250
Number of Nodes on External
Horizontal displacement, mm
0.75
0.7
0.65
0.6
0.55
0.5
0
50
100
150
200
250
Number of Nodes on External

◂**Fig. 1** **a** Geometry, dimensions, and boundary conditions of an arched roof reference tunnel, **b** The relationship between the number of nodes on the external boundary and the resulting vertical (top) and horizontal (bottom) displacements in the mesh sensitivity analysis

Saint Martin La Porte access adit, which runs along the Lyon-Turin Base Tunnel (Barla 2012). The study of numerical computation was performed using the Mohr–Coulomb failure criterion. Contact stiffness determines the stiffness of the interaction between the rock joint surfaces and the surrounding rock mass. The friction coefficient represents the resistance to sliding and accounts for the frictional forces between the contacting surfaces. The contact forces arise from the interaction between the rock joints and the rock mass and can be influenced by factors such as joint roughness and rock material properties.

3.1 Mesh Sensitivity Analysis

In order to obtain accurate analysis results in finite element analysis, it is highly recommended to perform mesh sensitivity analysis. This analysis helps prevent the negative impact caused by excessively long or thin elements on the accuracy of the analysis. Such thin elements typically have a high aspect ratio (Cami et al. 2018; He and Huang 2021). Within RS2D software, there is a built-in feature called "mesh and discretization settings" that aids users in identifying and resolving issues related to the finite element mesh. These settings include the type of mesh (graded), element type (4-Noded Quadrilateral), gradation factor (0.1), and the number of nodes on all excavations (200). Improper mesh configuration can lead to various problems such as solution non-convergence, terminated calculations, alert notifications, computation misconfigurations, and abnormal analysis results. To mitigate these issues, a sensitivity analysis was conducted to determine the optimal mesh size.

This involved establishing different models with varying mesh densities. During the analysis process, both vertical and horizontal displacements were carefully monitored while solving for elastic equilibrium, as depicted in Fig. 1b. When selecting the mesh size or density, several factors should be taken into consideration. A denser mesh provides a more precise representation of high-stress gradients (Rahmani et al. 2022; Maleki and Imani 2022; Maleki and Mir Mohammad Hosseini 2019). The accuracy of the results is directly related to the length of the elements. If different mesh sizes are required, it is recommended to transition gradually from denser to coarser meshes. Figure 1b shows that the model, running with 200 nodes on the external boundary, has reached a plateau. This indicates that further refining the mesh size does not significantly impact the results.

4 Results

4.1 Effect of Joint Dip Angle

The effects of seven joint set dipping angles (Table 1) on the tunnel's resilience are presented considering the WCR, RSR, FHR, induced stress, SF, SCF, and depth of failure zones into rock matrix surrounding the tunnel opening.

4.1.1 Wall Convergence Ratio (WCR)

The right wall of the tunnel moves laterally toward the left side of the tunnel (Fig. 2). The maximum right WCR (–0.0126%) takes place in the tunnel right border at zero distance from key point #3 (Fig. 1) and at a joint dip angle of 30°. The right WCR decreases as joint dip angle exceeds 30° to the minimum right WCR (–0.00284%) in the right wall of the tunnel at 2.5 m from key point #3 and a joint dip angle of 90°. Similarly, the left side of the tunnel moves laterally towards the tunnel's interior (Fig. 3). The maximum left WCR (0.0084%) occurs at zero distance from key point #2 and at a joint dip angle of 0°. The left WCR decreases as lateral displacement from key point #2 increases and as the joint dip angle increases until the minimum left WCR at 45° (–0.00048% at 2.5 m from key point #2). As the joint dip angle exceeds 45°, the left WCR increases to a maximum of 0.0078% at 90°. According to these results, the performance of tunnel walls is satisfactory (maximum WCR $\lesssim$1.5%). Figure 4 illustrates how the right and left tunnel walls move toward the center of the tunnel (Fig. 4).

4.1.2 Roof Sag (RSR) and Floor Heave (FHR) Ratios

Both the RSR and FHR decrease as joint dip angles increase (Fig. 5). The maximum value of the RSR

Table 1 Factors considered during the sensitivity analysis

Parameter/analysis	Effect of joint dip angle	Effect of joint spacing
Joint set dip angle, α (°)	0, 15, 30, 45, 60, 75, 90	30
Joint spacing (m)	5	0.5, 1.5, 3.5, 5
Stress ratio, k (unitless)	2.13	2.13
Tunnel depth (m)	50	50

Table 2 Geomechanical properties of rock mass and rock joints used in the 2-D (Barla et al. 2012; Abdellah et al. 2022)

Rock mass property	Limestone	Slate
Density (kg/m^3)	2,600	2,500
Compressive strength, (MPa)	30–250	100–200
Poisson's ratio, (unitless)	0.30	0.25
Tensile strength, (MPa)	0.60	0.10
Friction angle, (°)	40	35
Young's Modulus, (Gpa)	35	2.60
Cohesion, (MPa)	1	0.25
Dilation angle, (°)	20	15
Rock joints property (Das and Singh 2021; Abdellah et al. 2022)		
Normal stiffness, (Gpa)	21	
Shear stiffness, (Gpa)	15	
Friction angle (°)	39 (Sanei et al. 2015)	

(-0.0172%) and the FHR (–0.01174%) occur at a joint dip angle of 0° in the tunnel roof, at zero distance from key point #1 and in the tunnel floor from key point #4. The tunnel floor moves downward (negative displacement). Based on these results, the roof/back and floor of the tunnel are stable (maximum RSR and FHR ˂ 0.5%).

4.1.3 Major Induced Stress

Tensile induced stress occurs around the tunnel right and left wall (negative values in Fig. 6), whereas high compressive induced stress occurs around the tunnel roof and floor (positive values in Fig. 6). The UCS diminishes as joint dip angle increases and the maximum induced stress exhibits in the perimeter of the tunnel (i.e., at zero distance from the key points).

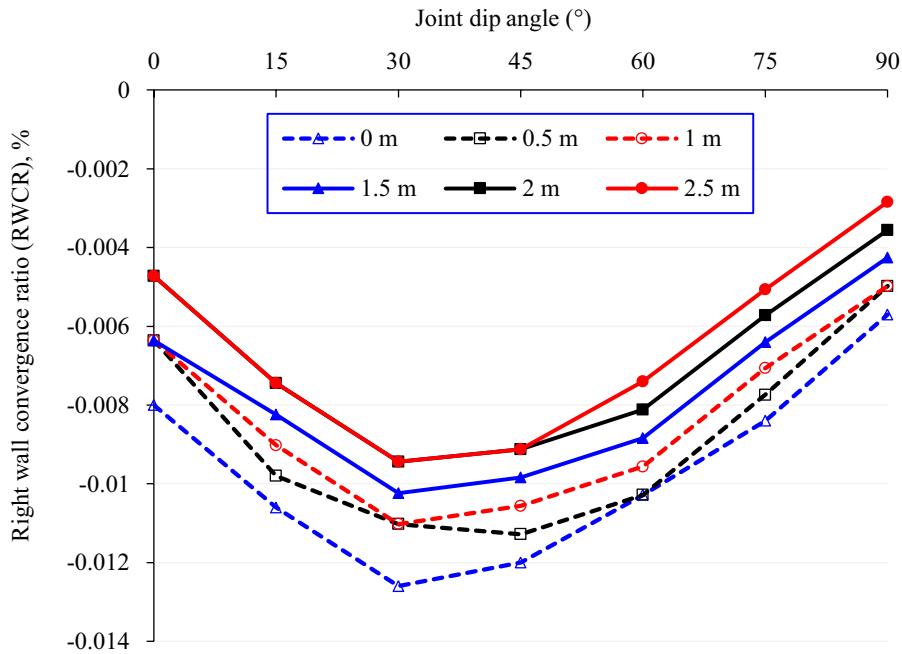

Fig. 2 Right wall convergence ratio at seven joint dip angles and six horizontal displacements from the tunnel's right periphery (reference point 3 in Fig. 1)

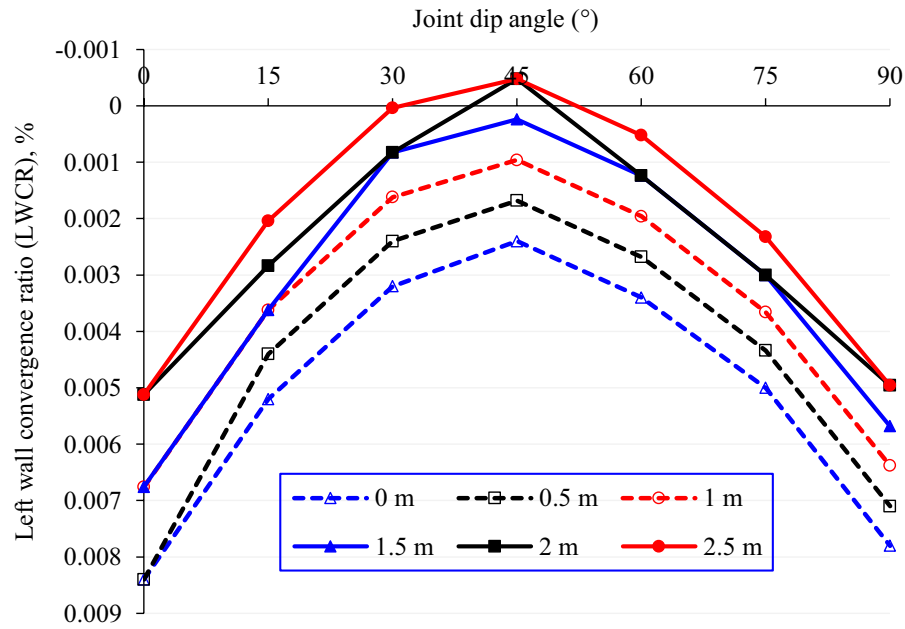

Fig. 3 Left wall convergence ratio at seven joint dip angles and six horizontal displacements from the tunnel's left side (reference point #2 in Fig. 1)

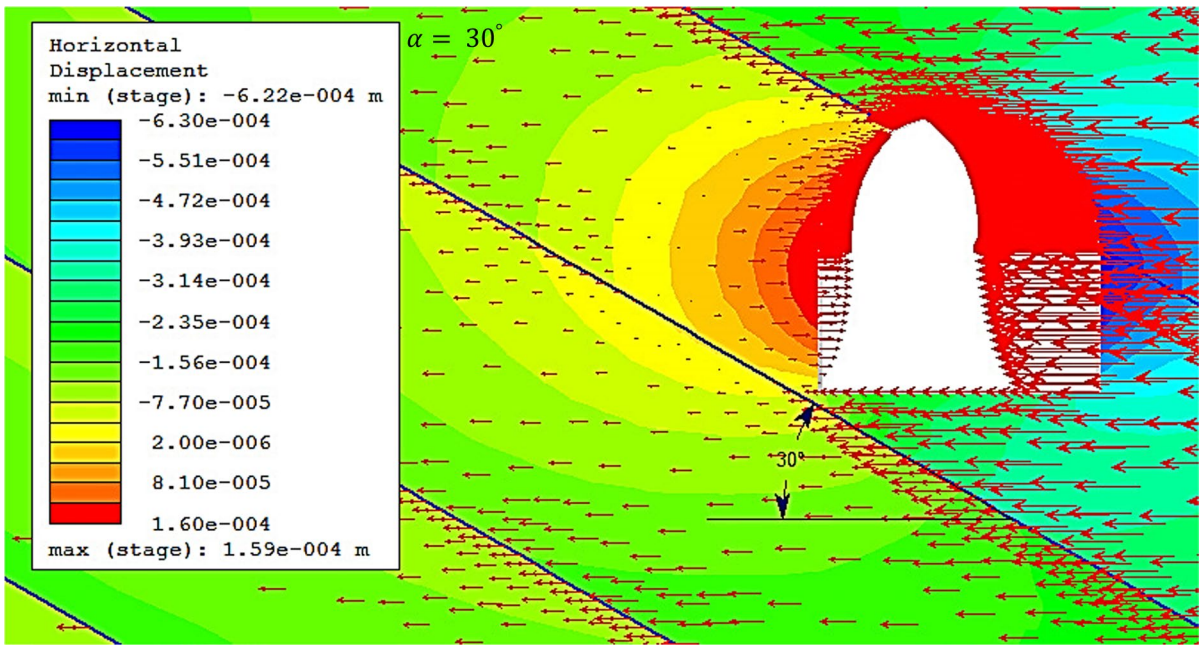

Fig. 4 Vectors of horizontal displacement contours around the tunnel at joint dip angle of 30°

4.1.4 Strength Factor (SF)

Figure 7 shows that the roof of the tunnel deteriorates (SF $^{<}$1) at all joint dip angles, whereas the floor of the tunnel only deteriorates at joint dip angles of 0 and 15°. The walls of the tunnel are stable (SF $^{>}$1) at all joint dip angles. In addition, the strength contours around the tunnel disconnects/splits after they are bisected by rock joints. The evaluation of rock tension using the Strength Factor (SF) method

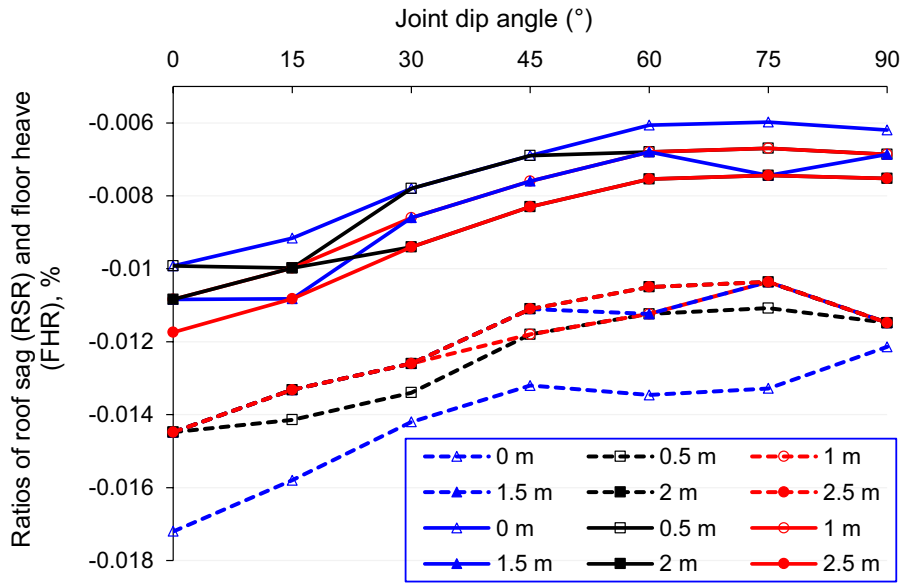

Fig. 5 Roof sag and floor heave ratios at seven joint dip angles, six vertical displacements from the tunnel back (dashed lines, Point #1) and six vertical displacements from the tunnel floor (solid lines, Point #4)

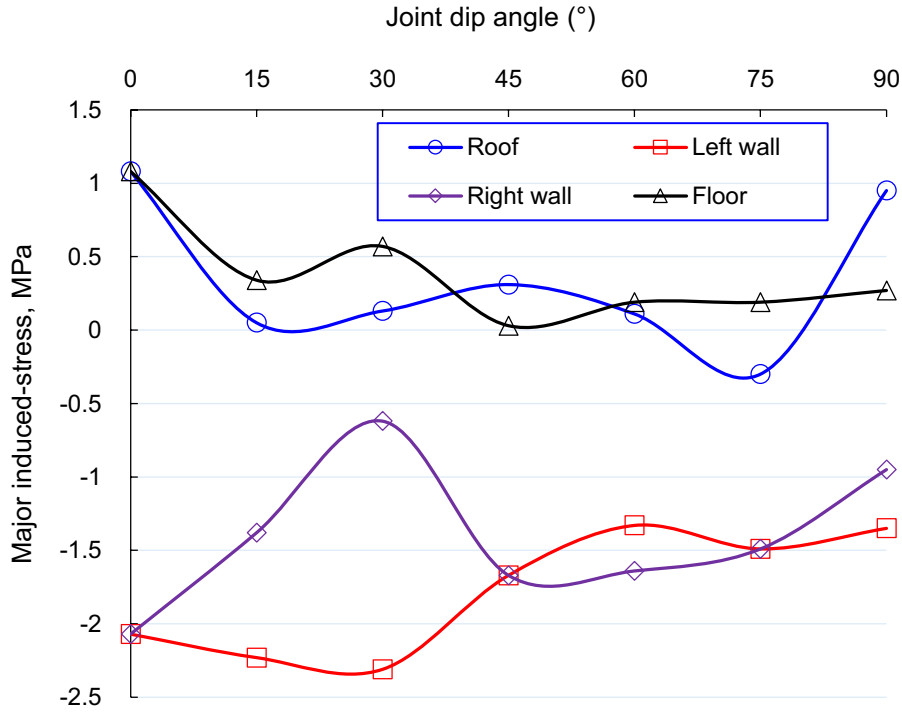

Fig. 6 Major induced stress around the tunnel boundary at seven joint dip angles

goes beyond the scope of this study. However, the following steps can be followed for conducting such an evaluation:

1. Determine the uniaxial compressive strength (UCS) of the rock material. This is typically obtained through laboratory tests.
2. Calculate the Strength Factor (SF) using the formula: $SF = \frac{UCS}{\sigma_3 - \sigma_t}$, where UCS is the uniaxial compressive strength, σ_3 is the minimum principal stress, and σ_t is the uniaxial tensile strength of the rock. The SF represents the ratio of the rock's

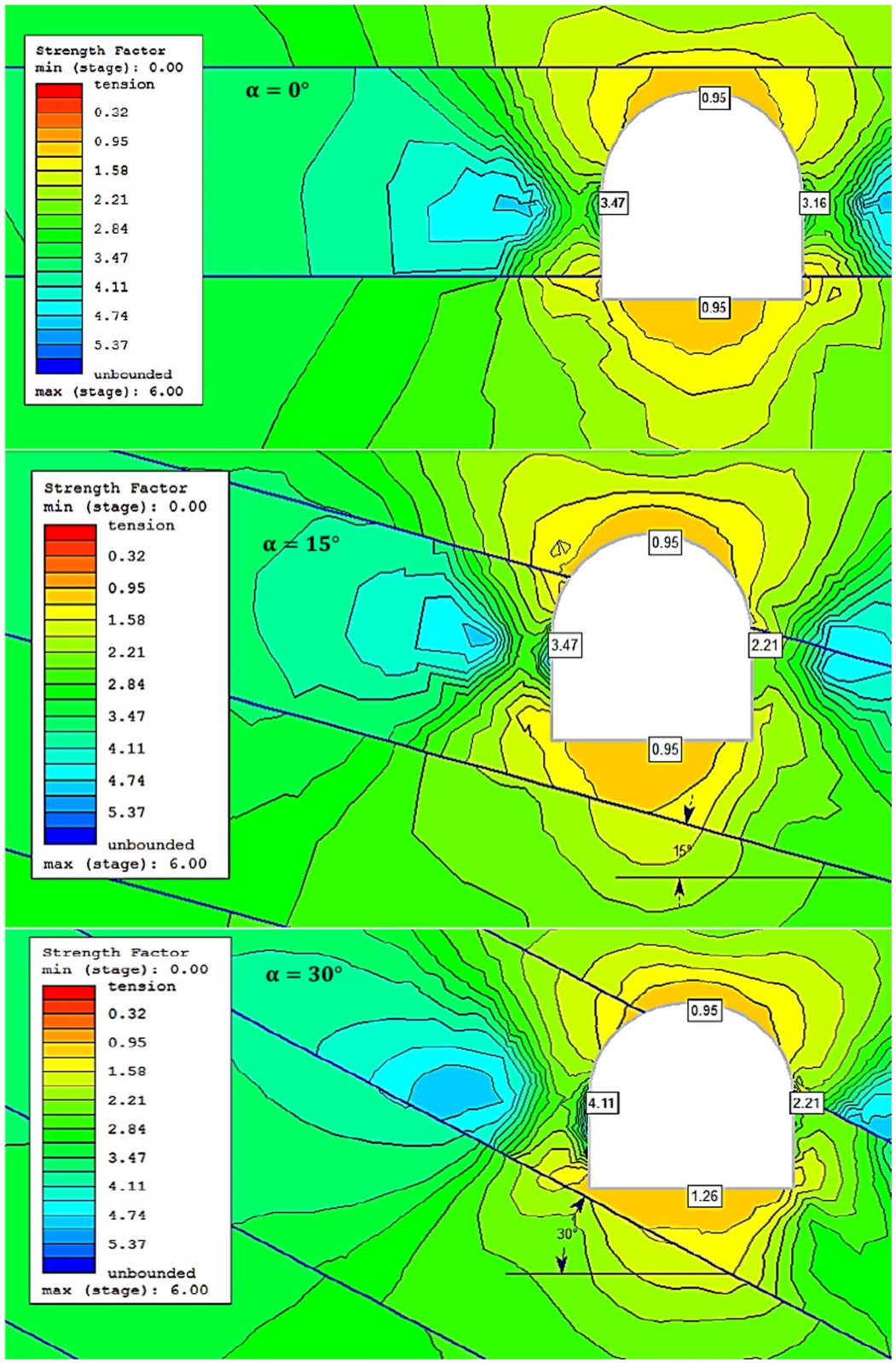

Fig. 7 Contours of strength factor at seven joint dip angles

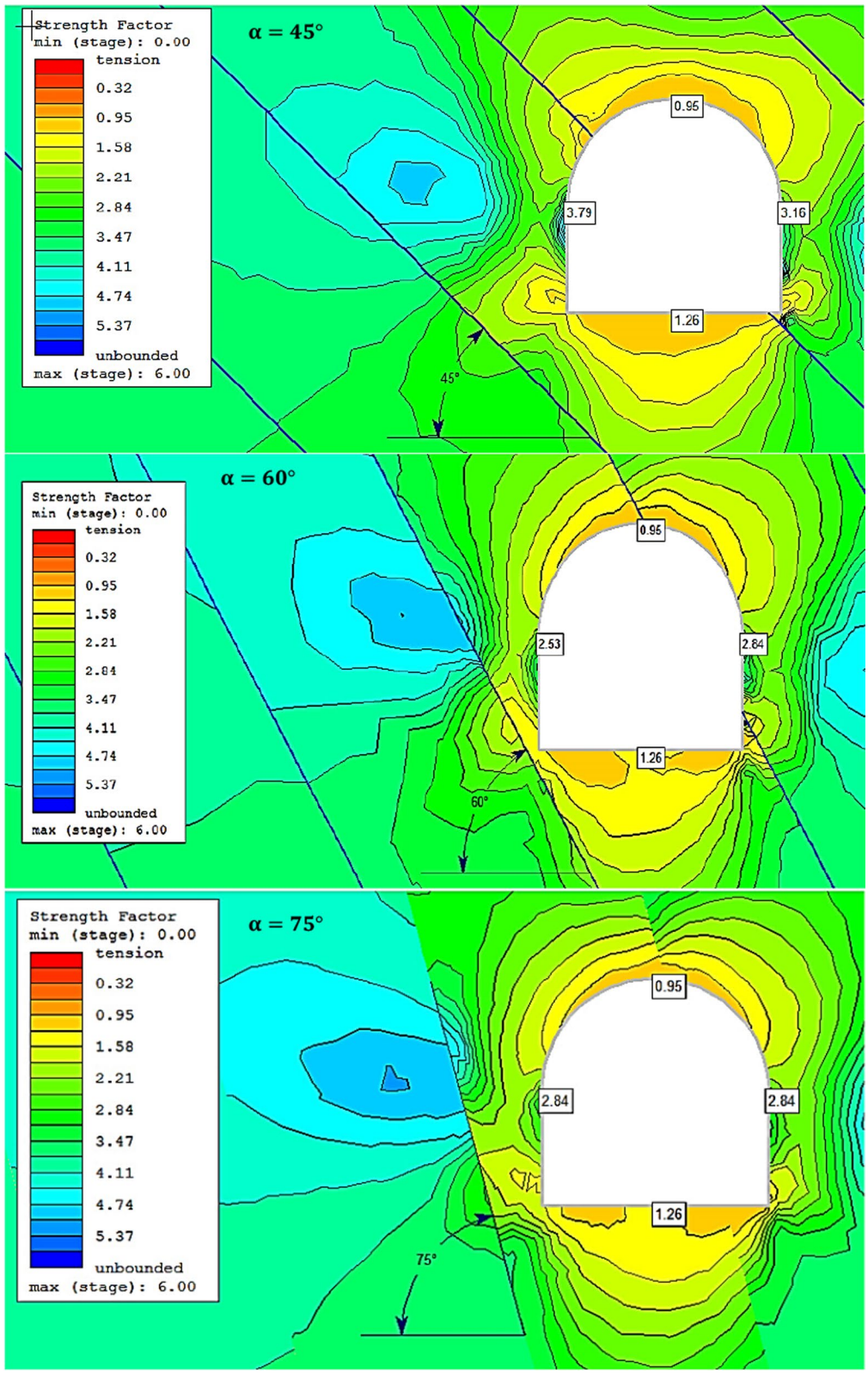

Fig. 7 (continued)

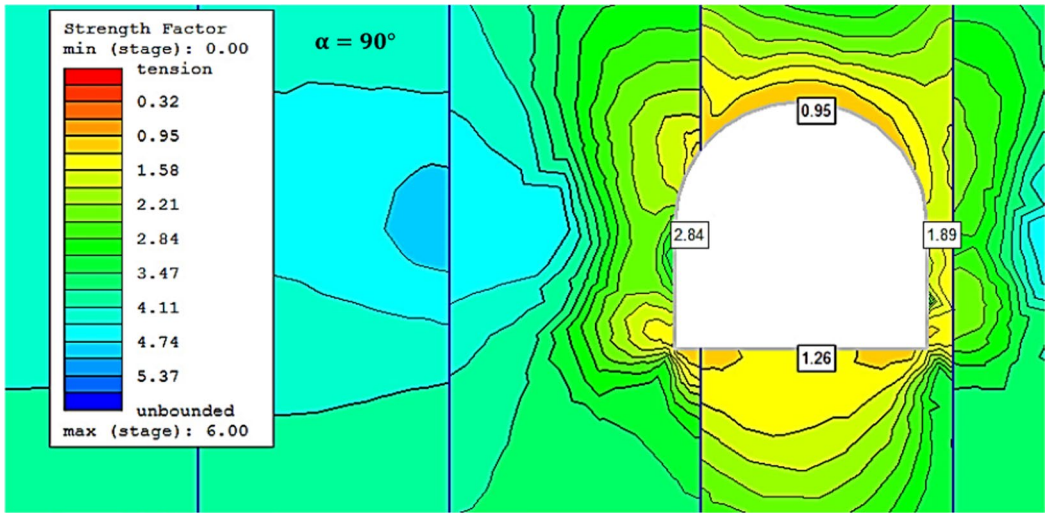

Fig. 7 (continued)

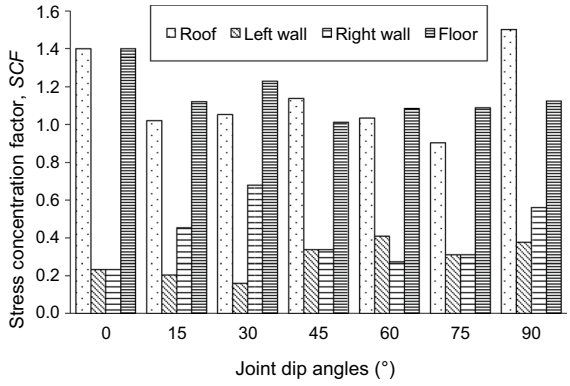

Fig. 8 Stress concentration factor around tunnel boundary at seven joint dip angles

strength to the difference between the minimum principal stress and the tensile strength.

3. Compare the SF value to a predefined threshold or criterion. If the SF is less than the threshold, it indicates that the rock is under tension and may be prone to failure.

4.1.5 Stress Concentration Factor (SCF)

High stress concentration develops around the tunnel's back (roof) and floor, whereas low stresses concentration take place around tunnel's shoulders (Fig. 8). The magnitude of stresses vary with joint dip angle. The highest SCF occurs at a joint dip angle of 90° in the back of the tunnel (1.50) and 0° in the floor of the tunnel (1.40). The objective of this study does not encompass the evaluation of rock tension using the Stress Concentration Factor (SCF) method. However, the following steps can be undertaken for such an evaluation:

1. Identify the presence of stress concentration points or regions in the rock mass. These could be caused by geological features, such as joints, faults, or other discontinuities.
2. Determine the Stress Concentration Factor (SCF) associated with each stress concentration point. The SCF represents the ratio of the maximum stress at the point of concentration to the average stress in the surrounding rock mass.
3. Assess the magnitudes of the SCFs. If the SCFs are significantly higher than unity, it indicates a localized increase in stress, which can lead to tension concentration and potential failure in the rock.

Both SF and SCF methods provide insights into the potential for rock tension and can help in assessing the stability of rock masses under different loading conditions.

4.1.6 Extent of Yielding Zones

Yielding varies with joint dip angle and only occurs around the tunnel's roof (back) and floor (Fig. 9). The minimum depths of yielding zones are 0 m (dip angle 0°) and 0.394 m (dip angle 60°), whereas the maximum depths of yielding zones are 0.917 m (dip angle 30°) and 0.765 m (dip angle 75°) around tunnel's

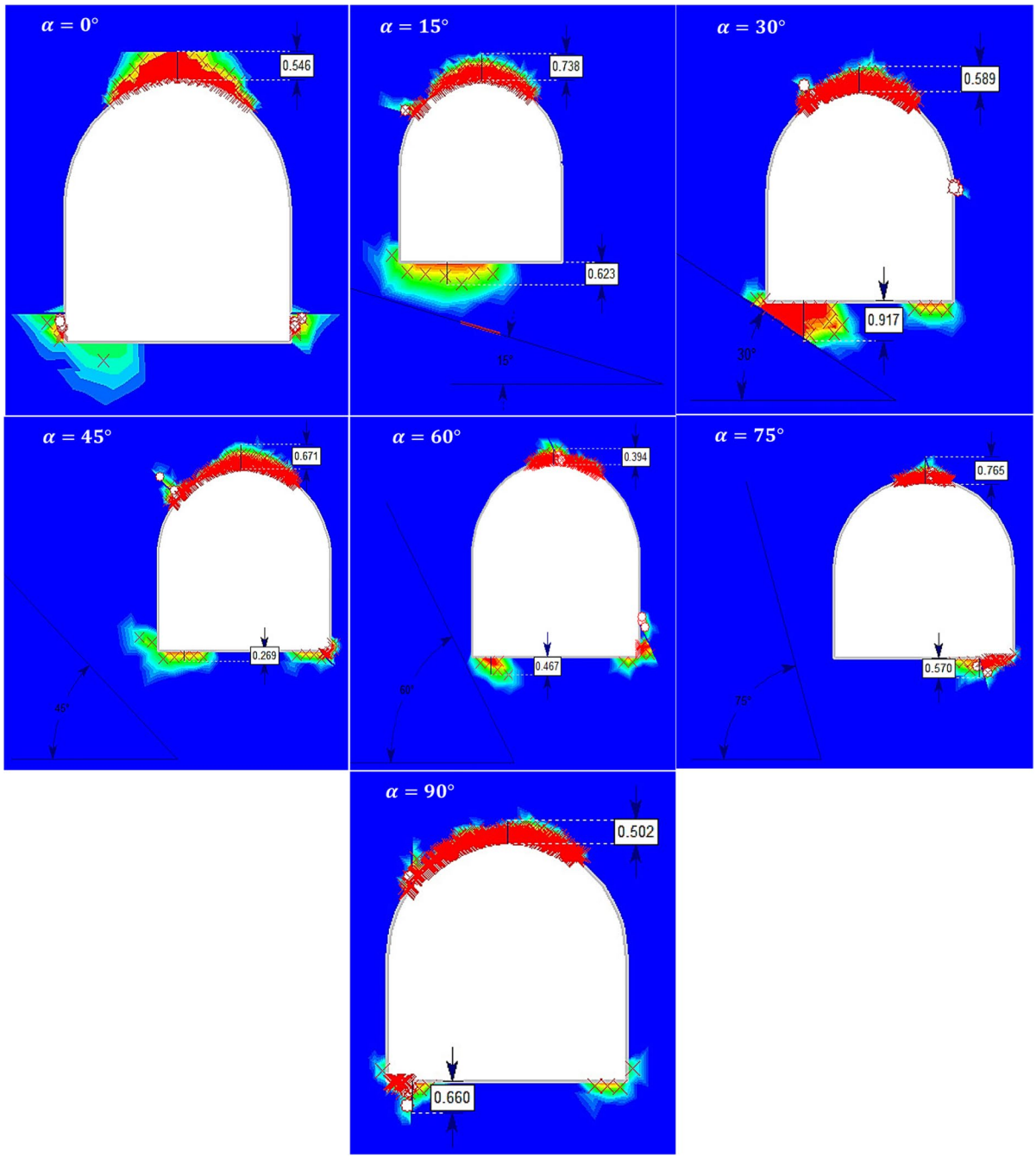

Fig. 9 The development of yielding zones around the boundary of the reference tunnel model at different joint dip angles, with a fixed joint spacing of 5 m

floor, and roof respectively. The performance of the tunnel is satisfactory (maximum extent of yielding zones ˂1.50 m).

4.2 Effect of Joint Spacing

The effects of four rock joint spacings (Table 1) are presented in terms of the WCR, RSR, FHR, induced stress, SF, SCF, and depth of failure zones in the rock matrix surrounding the tunnel opening.

4.2.1 Wall Convergence Ratio (WCR)

The WCR of tunnel walls decreases as joint spacing increases (Fig. 10). The maximum WCR occurs at 0.5 m joint spacing (–0.0546% and –0.0362% for right and left wall, respectively). The performance of the tunnel is satisfactory (WCR ˂1.50%). Both tunnel walls tend to move to the left (Fig. 11).

4.2.2 Roof Sag (RSR) and Floor Heave (FHR) Ratios

The RSR and FHR decrease as joint spacing increases (Fig. 12). The maximum RSR and FHR of –0.098% and –0.082%, respectively, occur at 0.5 m joint spacing.

4.2.3 Major Induced Stress

The major induced stress decreases as joint spacing increases (Fig. 13). The induced stress shifts from compressive (positive) to tensile (negative) stress around the tunnel walls as joint spacing increases, while the opposite occurs on the tunnel floor. The tunnel roof is surrounded by compressive induced stress.

4.2.4 Strength Factor (SF)

The rock mass contours across the tunnel show that, with the exception of 0.5 m joint spacing, the tunnel left wall, floor, and right wall are stable (SF > 1.0; Fig. 14). The roof of the tunnel is not stable (SF = 0.95) at any of the modelled joint spacings.

4.2.5 Stress Concentration Factor (SCF)

High stress concentrates around the tunnel roof at all joint spacings and around the tunnel floor at 3.5 and 5 m joint spacings (Fig. 15). In addition, high stress concentrates around the tunnel right wall at joint spacing 0.5 and 1.5 m, whereas it concentrates around the tunnel left wall at 0.5 m joint spacing.

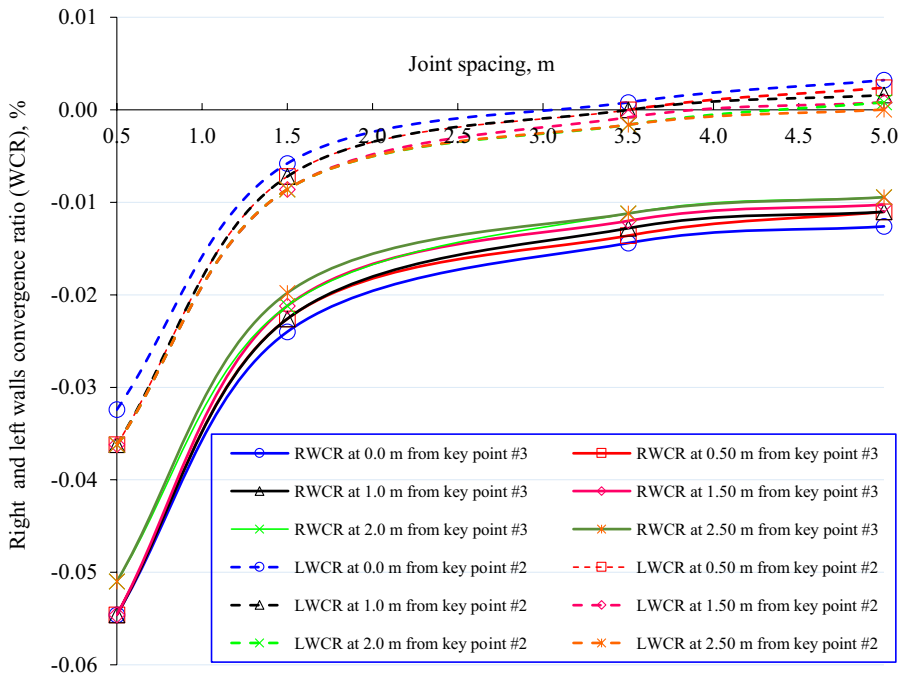

Fig. 10 Tunnel right (RWCR) and left (LWCR) walls convergence ratio at various joint spacings

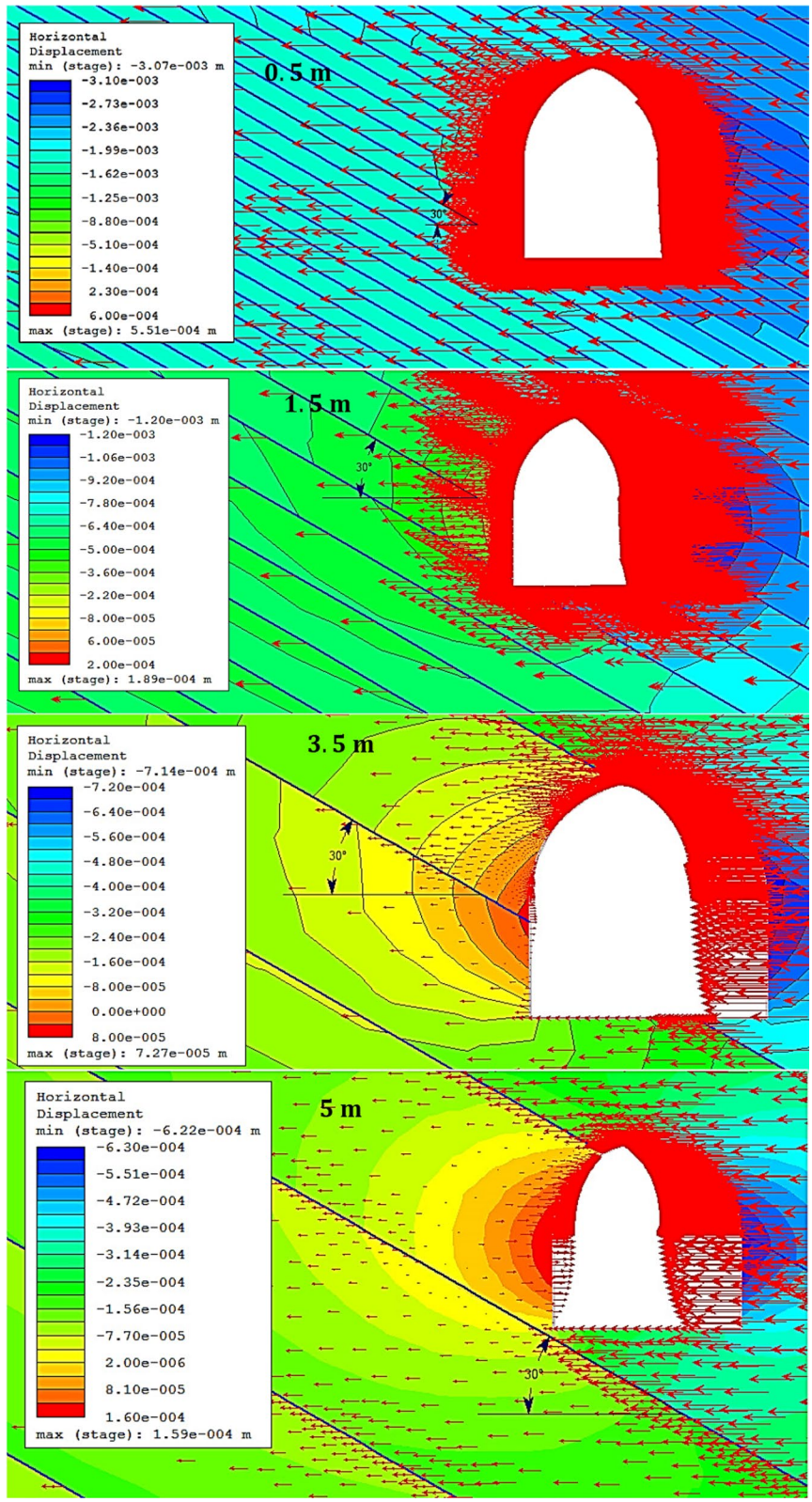

Fig. 11 Vectors of horizontal displacement contours showing reference tunnel model walls at joint dip angle of 30° and four joint spacings

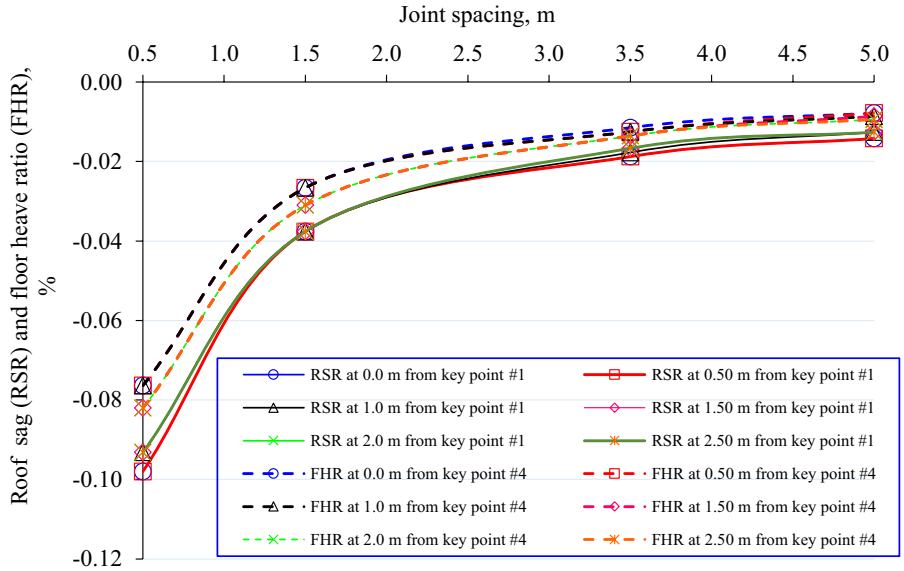

Fig. 12 Sag ratio of tunnel's roof (RSR) and heave ratio of tunnel's floor (FHR) at different joint spacings

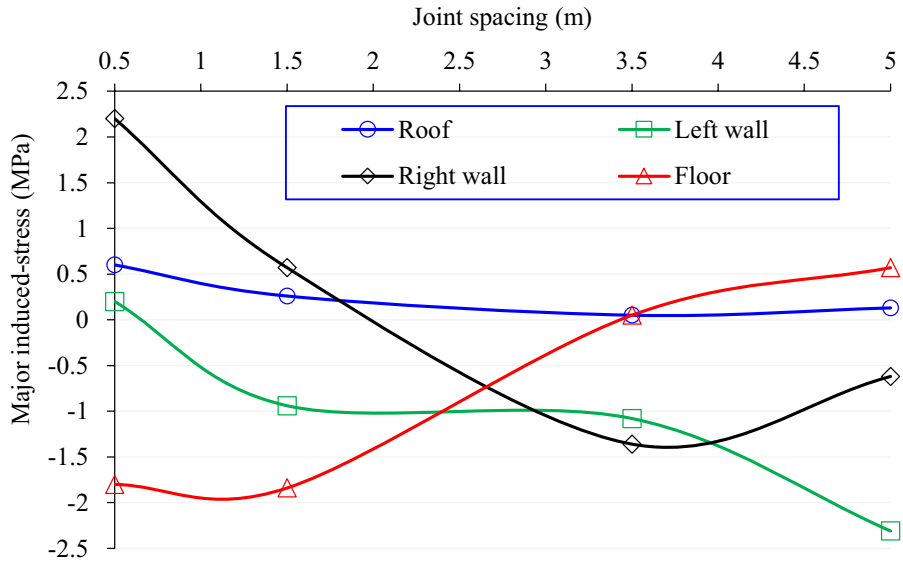

Fig. 13 Major induced-stress stress around the tunnel boundary at various joint spacings

4.2.6 Depth of Damage Zones

The failure zones occur in the tunnel's back and floor (Figs. 16 and 17). Based on the evaluation criterion, the functionality of the tunnel is acceptable (extent of yielding ˂1.50 m).

5 Discussion

The tunnel's behavior is investigated by conducting simulations with different orientations and spacings of rock joints. The focus of evaluating the tunnel's stability performance lies in analyzing stress

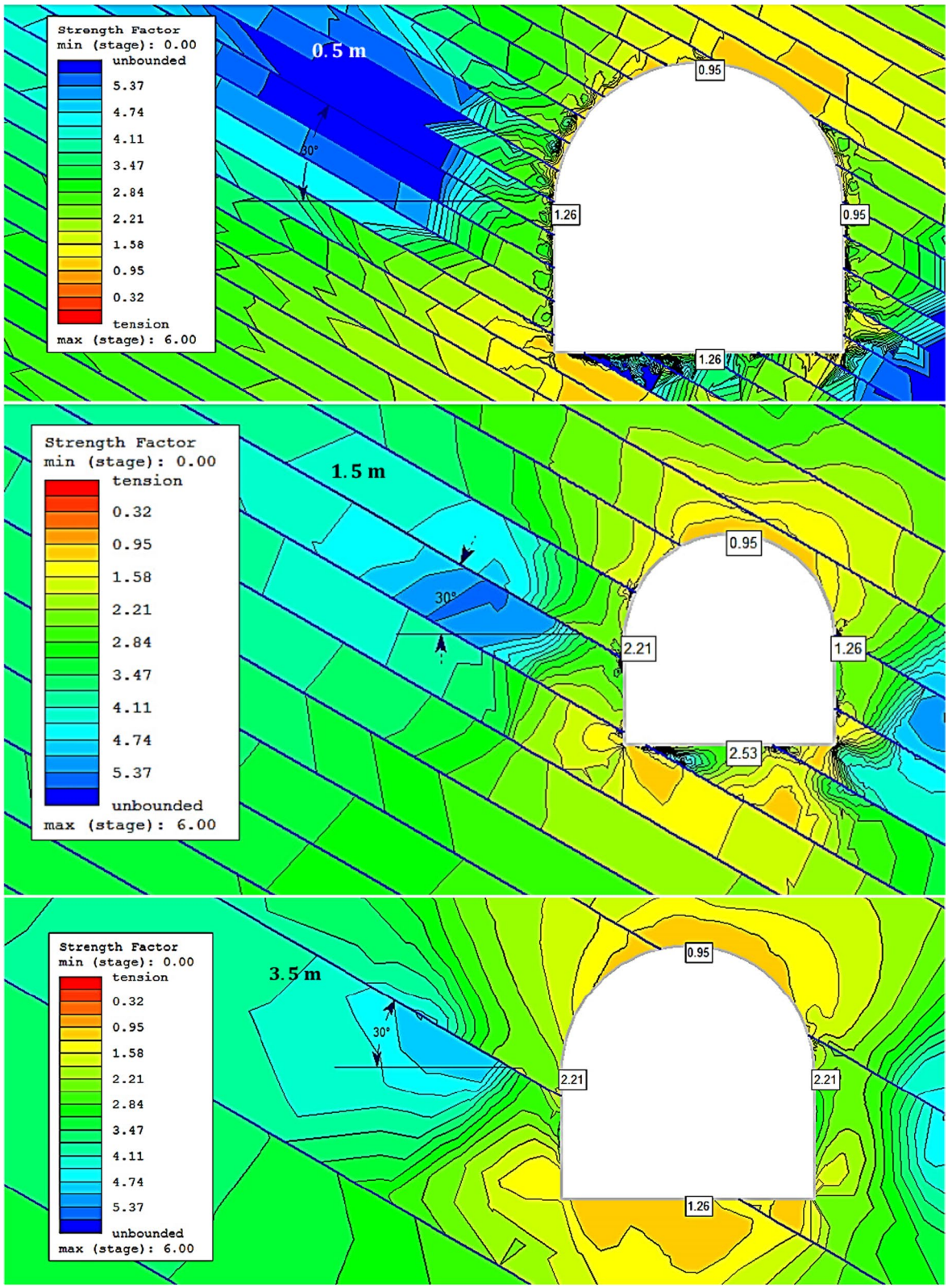

Fig. 14 Contours of strength factor (SF) at different joint spacings for the reference tunnel model at a joint dip angle of 30°

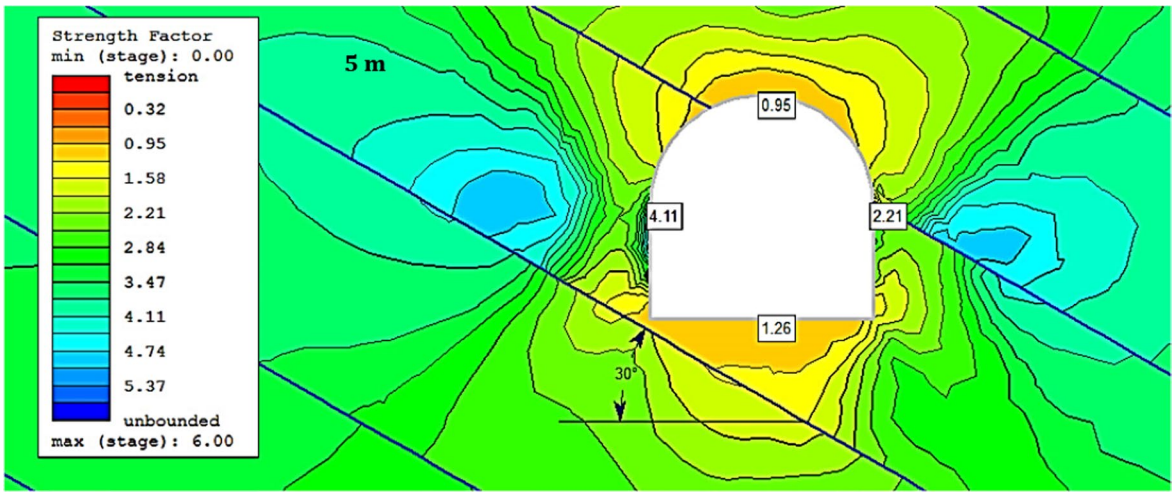

Fig. 14 (continued)

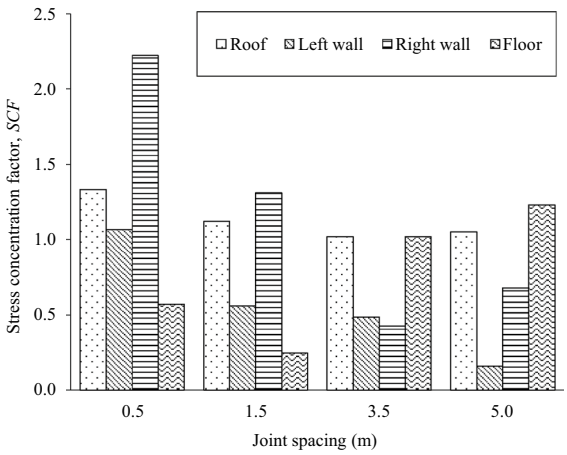

Fig. 15 Magnitude and location of stress concentration around the tunnel boundary

distribution, deformations (convergence), and the extent of Mohr–Coulomb yield zones along its boundaries. These metrics are used to interpret computational results.

To determine the level of satisfaction with the tunnel's stability performance, specific thresholds defined by the evaluation criteria are utilized. The selection of the evaluation criterion and its corresponding threshold relies primarily on the tunnel's intended purpose (application, expected lifespan), as well as observations from the field. It is worth noting that the computational results indicate minimal deformations at specified reference points along the tunnel's boundary, including wall convergence, roof sag, and floor heave. However, the monitoring of these deformations and the comparison with modeled values are carried out through the installation of borehole extensometers (MPBXs) at only three points, such as #1, #2, and #3.

On the other hand, when it comes to assessing the stress state, load cells are not integrated into the ground support system to measure stress redistribution on bolt heads and verify it against the modeled values. Consequently, establishing a single definitive threshold becomes challenging. Instead, a commonly employed criterion based on Mohr–Coulomb yield is employed to evaluate instability. The threshold for this criterion is determined using a rule of thumb approach, where resin grouted rebar is expected to withstand an axial load of 1 ton to 1.5 tons per 1-inch embedment extent of the bolt. Consequently, a minimum anchorage depth of 30 cm (12 inches) is established, as illustrated in Fig. 18.

In accordance with the rock support system employed in Canada, the primary rock support depth for the tunnel's roof and walls (for openings $\leq$ 18 ft in width) is set at 6 ft of rebar (1.8 m). Based on this length and the rule of thumb, the tunnel's instability occurs when the depth of damage zones exceeds 1.5 m, indicating insufficient embedment length ($<$30 cm) in the fresh rock mass beyond the yield zones.

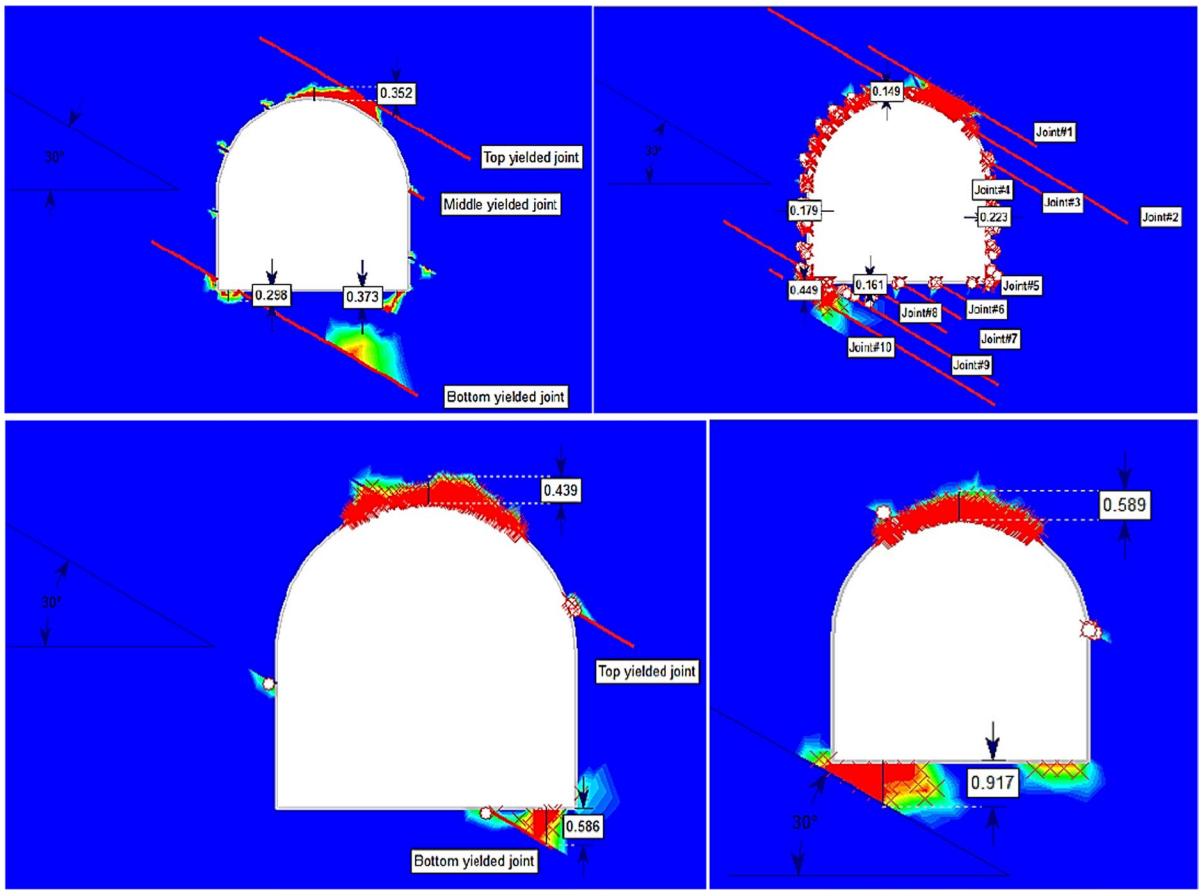

Fig. 16 Depth of damage zones contours around the borders of the reference model at four joint spacings (joint dip angle 30°)

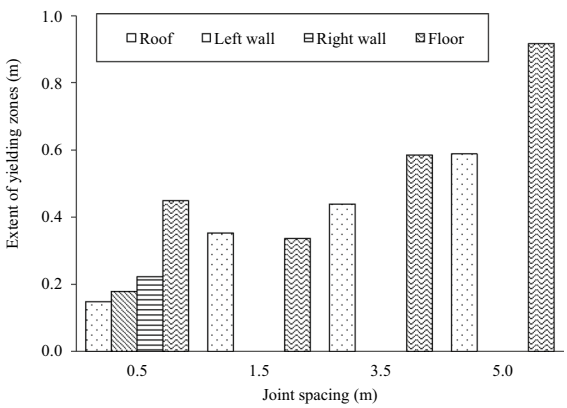

Fig. 17 Extent of yielding zones versus joint spacings

Case 1 examines the impact of different angles at which joints intersect on the stability of a tunnel entrance. The analysis reveals that as the joint dip angle surpasses 30°, the right wall convergence ratio (WCR) steadily decreases, reaching its minimum value (approximately -0.00284%) at a joint dip angle of 90°, specifically 2.5 m away from key point #3. Similarly, the left WCR decreases as the lateral displacement from key point #2 increases and the joint dip angle rises, reaching its minimum value of approximately -0.00048% at a joint dip angle of 45 degrees, also 2.5 m away from key point #2. However, as the joint dip angle exceeds 45°, the left WCR starts increasing and reaches a maximum value of 0.0078% at 90 degrees. These findings suggest that the tunnel walls remain structurally sound, with the highest WCR remaining below 1.5% (Adoko and Jiao 2013; Li and Liu 2015).

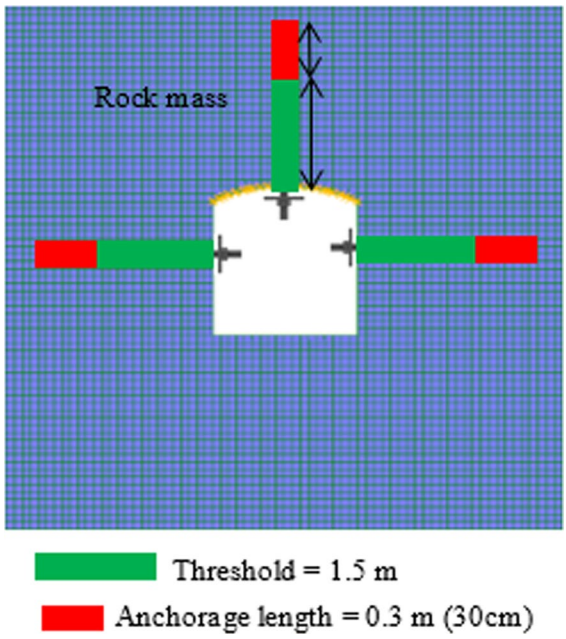

Fig. 18 Illustration of Mohr–Coulomb yield failure criterion

The downward movement of the tunnel floor (negative displacement) is observed, while the roof and back of the tunnel exhibit stability (maximum rock support ratio [RSR] and floor heave ratio [FHR] both below 0.5%). The uniaxial compressive strength (UCS) of the rock diminishes with increasing joint dip angle, and the highest induced stress occurs along the perimeter of the tunnel, specifically at zero distance from the key points. Additionally, the strength contours surrounding the tunnel become disjointed and split when intersected by rock joints. When the joints are perpendicular (90°), the tunnel's roof experiences the highest stress concentration (e.g., stress concentration factor [SCF] of 1.5), whereas in horizontal joints (0°), the tunnel's floor experiences the maximum stress concentration (e.g., SCF of 1.4).

The results demonstrate that the shortest failure zones in the rock mass (e.g., 0.394 m) occur in the tunnel's roof at joint dip angles of 60°, while the longest extension of failure zones into the rock mass (e.g., 0.765 m) occurs at joint dip angles of 75°. The maximum length of yielding zones (e.g., 0.917 m) in the tunnel's floor occurs at a joint dip angle of 30°. Nevertheless, the tunnel continues to function effectively, as the safe allowable length of yielding zones is 1.50 m. Alternatively, the effectiveness of the tunnel opening's resilience is evident through the minimum required anchorage length of rock support.

Case 2 delves into the influence of joint spacings on the stability of a tunnel entrance. The results indicate that the maximum convergence ratio (WCR) is observed at a joint spacing of 0.5 m, with the right wall of the tunnel experiencing the highest WCR (e.g., −0.0546%), followed by the left wall (e.g., −0.0362%). Despite this, the tunnel's overall performance remains satisfactory, as the WCR remains below 1.50%.

As the distance between joints increases, the induced stresses undergo a transition from compressive to tensile, particularly near the tunnel walls. Conversely, on the tunnel floor, tensile induced stresses are replaced by compressive induced stresses. The tunnel's roof, on the other hand, continues to bear compressive induced stress. When examining the strength contours of the rock mass, it becomes evident that the tunnel walls and floor exhibit stability across most joint spacings, except at a 0.5 m joint spacing. However, the tunnel's roof remains unstable regardless of the modelled joint spacings. Stress concentration areas surround the tunnel's roof at all joint spacings, while the tunnel floor experiences stress concentration at distances of 3.5 m and 5 m. Additionally, stress concentration areas cluster around the 0.5-m mark along the tunnel walls. The findings highlight that failure zones solely occur on the tunnel's roof and floor. Nonetheless, when assessed based on the evaluation criteria, the tunnel's functionality remains acceptable, as the extent of yielding remains below 1.50 m (Chung et al. 2006).

The results of this study indicate a relatively low sensitivity of wall convergence to variations in joint angle and spacing. This can be attributed to several factors. Firstly, the stiffness of the intact rock mass has a dominant influence on wall convergence, with the deformations primarily occurring within the stiffer intact rock rather than the joints. Additionally, stress redistribution within the rock mass during tunnel excavation helps distribute the deformation over a wider area, reducing the direct impact of joint angle and spacing on wall convergence. Moreover, the complex interaction between joints and the presence of other rock mass deformation mechanisms further contribute to the limited sensitivity of wall convergence to individual joint parameters. These findings suggest that while joint angle and spacing may have

some influence, other factors such as intact rock stiffness, stress redistribution, opening geometry (size and shape) and overall rock mass behavior play more significant roles in determining wall convergence in tunnel excavations (Yeung and Leong 1997; Jiang and Zhang 2011; Cai et al. 2019; Zhou et al. 2023).

5.1 The Validation of the Model through the Monitoring of Deformation (MPBX)

In order to monitor deformations in the rock mass along the surface of the tunnel, multi-point borehole extensometers (MPBX) are utilized (Hansmire 1978; Bayoumi 2011; Gholinia et al. 2022). These MPBX systems are employed specifically in the reference tunnel, with joint spacing of 5 m, joint dip angle of 30°, and positioned at zero meters from the tunnel boundary. The results of this monitoring act as proof for the RS2D numerical model. Figure 19 shows the locations of the three extensometers that have been put at the footwall drive #3156 junction, where the tunnel entrance is being built. MPBX#3 is specifically located in the right wall, MPBX#1 is situated in the intersection's ceiling, and MPBX#2 is located in the left wall. The measured horizontal relative deformations on the right wall and left wall are depicted in Figs. 20 and 21, respectively. Additionally, Fig. 22 presents the vertical relative displacement observed in the roof of the tunnel opening. Table 3 provides a concise overview of the maximum relative deformation values obtained from both the MPBX monitoring and RS2D calculations on the walls and roof surfaces of the tunnel openings.

The maximum monitored deformation on the tunnel's right wall (MPBX#3), as shown in Fig. 20, is −0.75 mm (0.015% convergence ratio). In comparison, Fig. 4 illustrates a deformation of −0.63 mm (0.0126% convergence ratio), and Fig. 2 presents a convergence ratio of 0.0126%. The difference between the measured and computed values is 0.12 mm (16%).

Likewise, Fig. 21 displays the maximum measured deformation on the tunnel's left shoulder using MPBX#2, which is 0.18 mm (0.0036% convergence ratio). This can be compared to a deformation of 0.16 mm (0.0032% convergence ratio) shown in Fig. 11 (or Fig. 3, which presents the computed value using RS2D). The difference between the observed and calculated values is 0.02 mm (11.11%).

In terms of the roof, Fig. 22 demonstrates a maximum measured deformation of −0.81 mm (equivalent to a sag ratio of 0.0162%). In contrast, Figs. 5 and 12

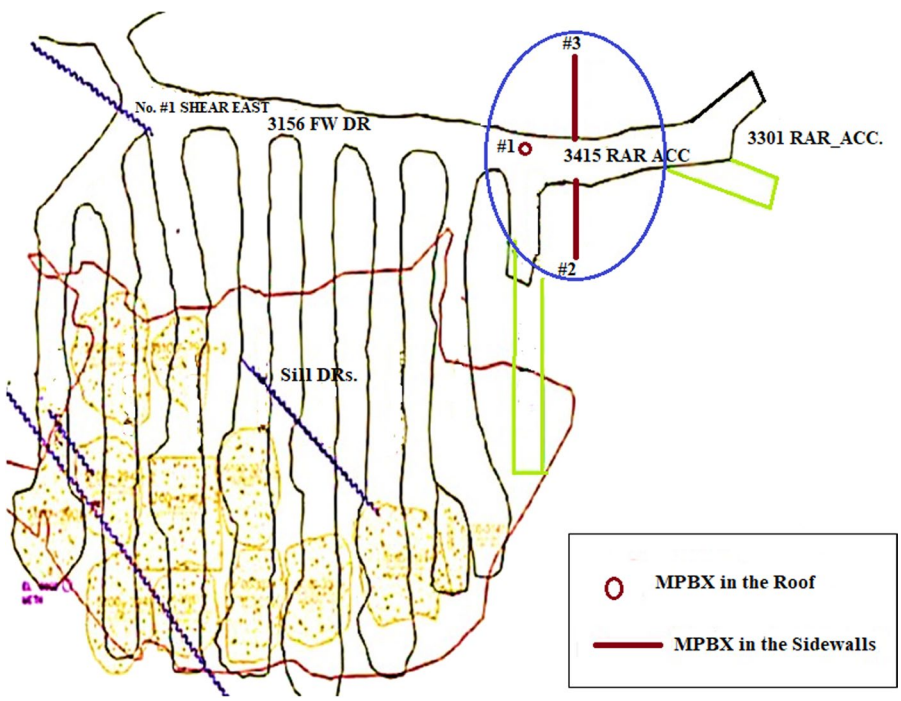

Fig. 19 Spatial arrangement of deformation monitoring points (MPBX) in the vicinity of intersection 3156

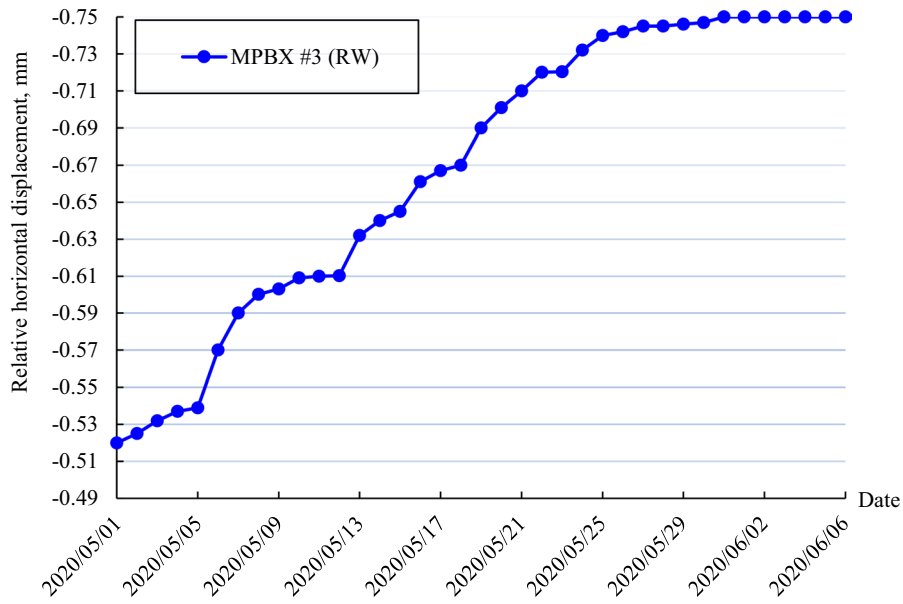

Fig. 20 The monitored relative horizontal displacement in the right wall of the tunnel following its full construction

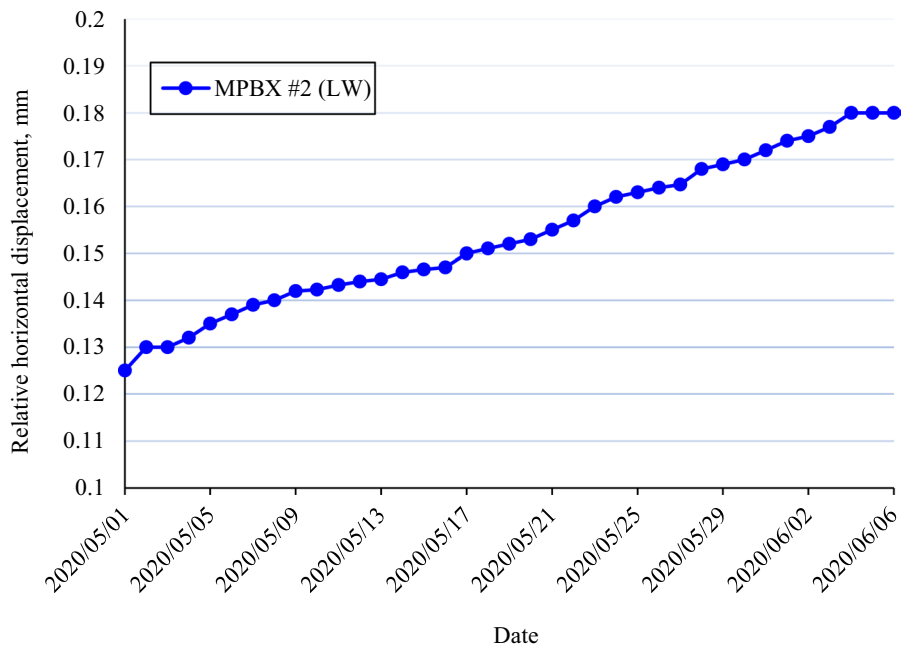

Fig. 21 The monitored relative horizontal displacement observed in the left wall of the tunnel after its complete construction

show a deformation of −0.71 mm (or a sag ratio of 0.0142%). The difference between the measured and computed sag ratios is 0.1 mm, corresponding to a sag ratio of 12.35%.

It is evident that both the measured and calculated deformations are very small, closely aligned, and insignificant. Consequently, the tunnel performance is deemed stable.

6 Conclusions

The numerical modeling study findings reveal the movement of both tunnel walls towards the center due to stress from the surrounding rock mass. The right wall experiences maximum convergence at a joint dip angle of 30°, while the minimum convergence occurs at 90°. Conversely, the left wall exhibits maximum

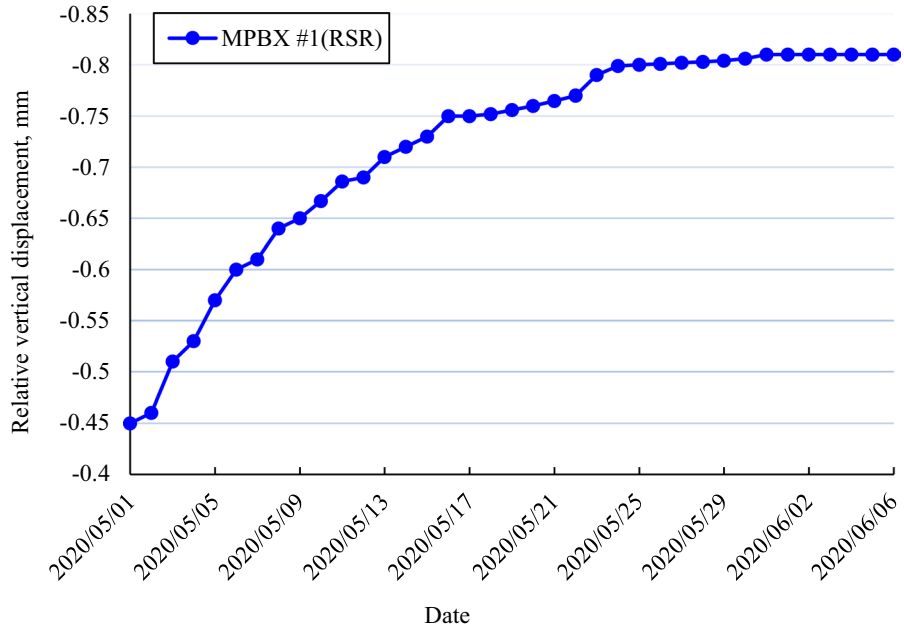

Fig. 22 The relative vertical displacement in the roof of the tunnel opening, as monitored after its full construction

Table 3 Comparison of computed and measured maximum deformations on the surface of the reference tunnel

MPBX Measured deformations, mm			RS2D Calculated deformations, mm			Difference, mm		
MPBX#3 RW (Fig. 20)	MPBX#2 LW (Fig. 21)	MPBX#1 Roof (Fig. 22)	RW (Figs. 2 & 4)	LW (Figs. 3 & 11)	Roof (Figs.5& 12)	RW	LW	Roof
-0.75	0.18	-0.81	-0.63	0.16	-0.71	-0.12	0.02	-0.1
Wall convergence and roof sag, % (Eqs. 1 & 2)			Wall convergence and roof sag, % (Eqs. 1 & 2)			Difference, %		
0.015	0.0036	0.0162	0.0126	0.0032	0.0142	16	11.11	12.35

convergence at a joint dip angle of 0° and minimum convergence at 45°. Moreover, the roof sag and floor heave show an inverse relationship with joint dip angles, decreasing as the angles increase. Similarly, the induced stress diminishes with higher joint dip angles.

The resilience of the rock mass near the tunnel roof and floor is compromised at joint dip angles of 0° and 15°. High stress concentrations are observed around the tunnel roof and floor, while low stress concentrations are concentrated around the walls. Additionally, yielding zones around the roof are insignificantly extended. As the spacing between joints increases, wall convergence/closure, roof deflection, heave of the floor ratios, and induced stress decrease. The strength of the rock mass deteriorates around the roof for all joint spacings, while it only deteriorates in the tunnel's right shoulder at a joint spacing of 0.5 m. High stress concentrations occur around the tunnel roof, while low stresses are concentrated around the walls and floor. The extent of yielding zones in the tunnel floor increases with joint spacing.

The novelty of this research lies in the application of this methodology to assess the impact of joints on tunnel stability, which can have significant implications across various industries. Specifically, our study's findings can be applied in mining operations for accessing mining blocks and facilitating efficient ore hauling. Additionally, the insights gained from this research can be utilized in the fields of tunnelling and civil engineering, particularly in the design and maintenance of transportation infrastructure.

By focusing on the effects of joint spacing and dip angles, this paper addresses a critical aspect of tunnel performance that has not been extensively explored in previous studies. It is believed that the comprehensive analysis presented in this research contributes to the existing body of knowledge in this field and provides practical insights for professionals involved in mining and civil engineering projects.

6.1 Similarities, Differences and Uniqueness

This study stands out in scholarly literature due to its unique approach and contributions. While there are several other comparable studies in the field, this research offers distinct features and contributions that set it apart.

6.1.1 Similarities

1. Topic of investigation: Like other studies, this research focuses on examining the stability of tunnels in relation to rock joint orientations and spacing.
2. Utilization of computational tools: Similar to other studies, this research employs computational tools to simulate and analyze the behavior of tunnels under different conditions.

6.1.2 Differences and Uniqueness

1. Comprehensive evaluation metrics: This study sets itself apart by utilizing a wide range of evaluation metrics, including wall convergence/closure ratio, roof deflection and floor uplift ratios, induced stress, strength factor, strength concentration factor, and spread of damage zones. The comprehensive nature of these metrics provides a more holistic understanding of tunnel stability.
2. Threshold framework: Unlike many other studies, this research establishes specific thresholds for the evaluation measures. These thresholds serve as a framework to assess the computational results and determine the stability of the tunnel. This approach adds an element of quantifiability and enables a more objective evaluation.
3. Emphasis on uniqueness: From the outset, this study emphasizes its uniqueness and distinguishes itself from another published research. By highlighting the novel aspects of the study, such as the evaluation metrics and threshold framework, it asserts its special contribution to the existing body of literature.

Overall, what sets this study apart is its comprehensive evaluation approach, the establishment of specific thresholds, and its emphasis on uniqueness. By offering a distinct perspective and framework for assessing tunnel stability, this research contributes to the existing knowledge in the field.

6.1.3 Limitation and Recommendation

The scope of this study is confined to a two-dimensional analysis, which may not fully capture the precise geometry of the tunnel opening. To obtain a more accurate representation, it is essential to incorporate a three-dimensional analysis that considers the complete geometry of the opening.

To enhance the analysis further, it is advisable to expand the parametric stability analysis by including additional joint geometric properties like stiffness, roughness, and friction. Furthermore, considering different stress ratios and depths would contribute to a more comprehensive understanding of the system.

Additionally, it is recommended to employ probabilistic analysis to address the inherent uncertainty, variability, and heterogeneity associated with the properties of the rock mass. This approach will provide insights into probabilistic behavior and better inform the assessment and decision-making processes.

Acknowledgements The authors wish to convey their appreciation for the revision and editing services offered by the Canadian English Centre (CEC), Scarborough, Ontario, Canada.

Funding The authors have not disclosed any funding.

Data availability Enquiries about data availability should be directed to the authors.

Declarations

Conflicts of interest The author declares no conflict of interest.

References

Abdellah WRE (2015) Practical application of stochastic methods in geotechnical engineering. J Eng Sci (JES) 43:57–70. https://doi.org/10.21608/jesaun.2015.115147

Abdellah WRE (2015) Numerical modelling stability analyses of haulage drift in deep underground mines. J Eng Sci 43:71–81. https://doi.org/10.21608/jesaun.2015.115148

Abdellah W, Mitri HS, Thibodeau D, Moreau-Verlaan L (2014) Stability of mine development intersections—a probabilistic analysis approach. Can Geotech J 51:184–195. https://doi.org/10.1139/cgj-2013-0123

Abdellah WR, Ali MA, Yang HS (2018) Studying the effect of some parameters on the stability of shallow tunnels. J Sustain Min 17:20–33. https://doi.org/10.1016/j.jsm.2018.02.001

Abdellah WR, Haridy AKA, Mohamed AK, Kim JG, Ali MA (2022) Behaviour of horseshoe-shaped tunnel subjected to different in situ stress fields. Appl Sci 12(11):5399. https://doi.org/10.3390/app12115399

Abdellah W, Mitri HS (2016) Estimating the probability of unsatisfactory performance associated with the instability of mine developments. In: the 3rd international symposium on mine safety science and engineering, Montreal, Canada. August 13–19, 2016

Adoko AC, Jiao YY, Wu L, Wang H, Wang ZH (2013) Predicting tunnel convergence using multivariate adaptive regression spline and artificial neural network. Tunn Undergr Sp Technol 38:368–376. https://doi.org/10.1016/j.tust.2013.07.023

Aksoy CO, Aksoy G, Guney A, Ozacar V, Yaman H (2020) Influence of time-dependency on elastic rock properties under constant load and its effect on tunnel stability. Geomech Eng 20:1–7. https://doi.org/10.12989/gae.2020.20.1.001

Barla G, Debernardi D, Sterpi D (2012) Time-dependent modeling of tunnels in squeezing conditions. Int J Geomech 12:697–710. https://doi.org/10.1061/(ASCE)GM.1943-5622.0000163

Bayoumi A (2011) On the evaluation of settlement measurements using borehole extensometers. Geotech Geol Eng 29(1):75–90. https://doi.org/10.1007/s10706-010-9352-2

Berisavljević Z, Berisavljević D, Čebašek V, Rakić D (2015) Slope stability analyses using limit equilibrium and strength reduction methods. Građevinar 67:975–983. https://doi.org/10.14256/JCE.1030.2014

Brady BHG (1977) An analysis of rock behaviour in an experimental stoping block at the Mount Isa Mine Queensland, Australia. Int J Rock Mech Min Sci Geomech Abstr 14:59–66. https://doi.org/10.1016/0148-9062(77)90197-8

Brady B, Lorig L (1988) Analysis of rock reinforcement using finite difference methods. Comp Geotech 5:123–149. https://doi.org/10.1016/0266-352X(88)90042-0

Brinkgreve RBJ, Bakker HL (1991) Non-linear finite element analysis of safety factors. In: proceedings of the 7th international conference on comp methods and advances in geomechanics, Cairns, Australia, May 1977

Cai J, Du G, Ye H, Lei T, Xia H, Pan H (2019) A slate tunnel stability analysis considering the influence of anisotropic bedding properties. Adv Mater Sci Eng 1:1–17. https://doi.org/10.1155/2019/4653401

Cami B, Javankhoshdel S, Bathurst RJ, Yacoub T (2018) Influence of mesh size, number of slices, and number of simulations in probabilistic analysis of slopes considering 2D spatial variability of soil properties. IFCEE 2018:186–196

Chen GH, Zou JF, Qian ZH (2019) An improved collapse analysis mechanism for the face stability of shield tunnel in layered soils. Geomech Eng 17:97–107. https://doi.org/10.12989/gae.2019.17.1.097

Chinaei F, Ahangari K, Shirinabadi R (2021) Hoek-Brown failure criterion for damage analysis of tunnels subjected to blast load. Geomech Eng 26:41–47

Chung HS, Chun BS, Kim BH, Lee YJ (2006) Measurement and analysis of long-term behavior of Seoul metro tunnels using the automatic tunnel monitoring systems. Tunn Undergr Sp Technol Incorporat Trenchless Technol Res 21(3):316–317. https://doi.org/10.1016/j.tust.2005.12.032

Das R, Sing T (2021) Effect of closely spaced, non-persistent ubiquitous joint on tunnel boundary deformation: a case study from Himachal Himalaya. Geotech Geol Eng 39:2447–2459. https://doi.org/10.1007/s10706-020-01637-3

Dong J, Zhong S, Wang HI, Wu ZH (2020) Dynamic response characteristics of crossing tunnels under heavy-haul train loads. Geomech Eng 20:103–112. https://doi.org/10.12989/gae.2020.20.2.103

Edelbro C (2010) Different approaches for simulating brittle failure in two hard rock mass cases: a parametric study. Rock Mech Rock Eng 43:151–165. https://doi.org/10.1007/s00603-008-0025-x

Eman AE, Attia G, Fawzy H, Abdel Hafez K (2013) Behavior of different shapes of twin tunnels in soft clay soil. Int J Eng Innov Technol 2: 298–302. https://www.ijeit.com/vol%202/Issue%207/IJEIT1412201301_53.pdf

Everling G (1964) Model study of rock-joint deformation. Int J Rock Mech Min Sci Geomech 1:319–326

Fan H, Li L, Liu H, Shib Sh, Huc J, Zhou Sh (2021) Advanced stability analysis of the tunnels in jointed rock mass based on TSP and DEM. KSCE J Civ Eng 25:1491–1503. https://doi.org/10.1007/s12205-021-0170-2

Gholinia A, Nikkhah M, Naderi R (2022) Validation of borehole extensometers results in geotechnical monitoring. Environ Earth Sci 81(11):312. https://doi.org/10.1007/s12665-022-10422-9

Ghorbani K, Zahedi M, Asaadi A (2015) Effects of statistical distribution of joint trace length on the stability of tunnel excavated in jointed rock mass. Int J Min Geo Eng 49:289–296

Goodman RE, Heuze HE, Bureau GJ (1972) On modeling techniques for the study of tunnels in jointed rock. In: proceedings of the 14th symposium on rock mechanics, University Park, Pennsylvania, USA, June 1972

Guntumadugu DR (2013) Methodology for the design of dynamic rock supports in burst prone ground.

Dissertation, McGill University, Montreal, Quebec, Canada
Hammah RE, Yacoub TE, Corkum BC (2005) The shear strength reduction method for the generalized Hoek-Brown criterion. The 40th U.S. Symposium on Rock Mechanics (USRMS), Anchorage, Alaska, USA, June 2005
Hansmire WH (1978) Suggested methods for monitoring rock movements using borehole extensometers. Int J Rock Mech Min Sci 15(6):305–317. https://doi.org/10.1016/0148-9062(78)91471-7
Hao YH, Azzam R (2005) The plastic zones and displacements around underground openings in rock masses containing a fault. Tunn Undergr Sp Technol 20:49–61. https://doi.org/10.1016/j.tust.2004.05.003
He Y, Huang W (2021) Mesh sensitivity analysis for finite element solution of linear elliptic partial differential equations. arXiv preprint arXiv:2111.10935.10.48550/arXiv.2111.10935
Heidarzadeh S, Saeidi A, Rouleau A (2021) The damage-failure criteria for numerical stability analysis of underground excavations: a review. Tunn Undergr Sp Technol 107:103633. https://doi.org/10.1016/j.tust.2020.103633
Rocscience Inc. (2016) Rock-Soil, 2D finite element software, Rocscience Inc., Toronto. https://www.rocscience.com/software/rs2
Jaeger JC, Cook NGW (1979) Fundamentals of rock mechanics, 3rd edn. Halsted Press, NY, USA
Jeon S, Kim J, Seo Y, Hong C (2004) Effect of a fault and weak plane on the stability of a tunnel in rock—a scaled model test and numerical analysis. Int J Rock Mech Min Sci 41:658–663. https://doi.org/10.1016/j.ijrmms.2004.03.115
Jia P, Tang CA (2008) Numerical study on failure mechanism of tunnel in jointed rock mass. Tunn Undergr Sp Technol 23:500–507. https://doi.org/10.1016/j.tust.2007.09.001
Jiang JP, Zhang YS (2011) Study on the influence of dip angles of normal fault on tunnel surrounding rocks in the fault footwall. J Min Safety Eng 28(4):596–602
Jiang Y, Tanabashi Y, Li B, Xiao J (2006) Influence of geometrical distribution of rock joints on deformational behavior of underground opening. Tunn Undergr Sp Technol 21:485–491. https://doi.org/10.1016/j.tust.2005.10.004
Kim NY, Park DH, Jung HS, Kim MI (2020) Deformation characteristics of tunnel bottom after construction under geological conditions of long-term deformation. Geomech Eng 21:171–178. https://doi.org/10.12989/gae.2020.21.2.171
Kirsch G (1898) Die theorie der elastizitat und die bedörfnisse der festigkcitslchre. Veit Ver Deut Ing 42:797–807
Kulatilake PHSW, Wu Q, Yu Z, Jiang F (2013) Investigation of stability of a tunnel in a deep coal mine in China. Int J Min Sci Technol 23:579–589. https://doi.org/10.1016/j.ijmst.2013.07.018
Ladanyi B. (1974) Use of the long-term strength concept in the determination of ground pressure on tunnel linings. In: Proceedings of the 3rd International Society of Rock Mechanics Congress, Denver, USA
Lee JS, Sagong M, Yoo J, You K (2012) Analytical modeling and experimental verification of a tunnel with joint sets. Int J Rock Mech Min Sci 50:56–64. https://doi.org/10.1016/j.ijrmms.2011.12.011
Lee KH, Lee IM, Shin YJ (2020) Quantitative assessment of depth and extent of notch brittle failure in deep tunneling using inferential statistical analysis. Geomech Eng 21:201–206. https://doi.org/10.12989/gae.2020.21.2.201
Li YH, Xu S-d, Liu JP (2015) A new convergence monitoring system for tunnel or drift based on draw-wire displacement sensors. Tunn Undergr Space Technol 49:92–97. https://doi.org/10.1016/j.tust.2015.04.005
Li HB, Liu MC, Xing WB, Shao S, Zhou JW (2017) Failure mechanisms and evolution assessment of the excavation damaged zones in a large-scale and deeply buried underground powerhouse. Rock Mech Rock Eng 50:1883–1900. https://doi.org/10.1007/s00603-017-1208-0
Li B, Fu Y, Hong Y, Cao Z (2021) Deterministic and probabilistic analysis of tunnel face stability using support vector machine. Geomech Eng 25:17–30. https://doi.org/10.12989/gae.2021.25.1.017
Lukic DC, Zlatanovic EM, Jokanovic IM (2020) Tunnel lining load with consideration of the rheological properties of rock mass and concrete. Geomech Eng 21:53–62. https://doi.org/10.12989/gae.2020.21.2.053
Madkour H (2012) Parametric analysis of tunnel behavior in jointed rock. Ain Shams Eng J 3:79–103. https://doi.org/10.1016/j.asej.2012.01.002
Maghous S, Bernaud D, Fréard J, Garnier D (2008) Elasto-plastic behavior of jointed rock masses as homogenized media and finite element analysis. Int J Rock Mech Min Sci 45:1273–1286. https://doi.org/10.1016/j.ijrmms.2008.01.008
Maleki M, Imani M (2022) Active lateral pressure to rigid retaining walls in the presence of an adjacent rock mass. Arab J Geosci 15(2):152. https://doi.org/10.1007/s12517-022-09454-z
Maleki M, Mir Mohammad Hosseini SM (2019) Seismic performance of deep excavations restrained by anchorage system using quasi static approach. J Seismol Earthq Eng 21(2):11–21. https://doi.org/10.48303/JSEE.2019.240810
Maleki M, Mir Mohammad Hosseini SM (2022) Assessment of the Pseudo-static seismic behavior in the soil nail walls using numerical analysis. Innov Infrastruct Solut 7(4):262. https://doi.org/10.1007/s41062-022-00861-5
Maleki M, Nabizadeh A (2021) Seismic performance of deep excavation restrained by guardian truss structures system using quasi-static approach. SN Appl Sci 3:1–17. https://doi.org/10.1007/s42452-021-04415-9
Maleki M, Khezri A, Nosrati M, Hosseini SM (2023) Seismic amplification factor and dynamic response of soil-nailed walls. Modeling Earth Syst Environ 9(1):1181–1198. https://doi.org/10.1007/s40808-022-01543-y
Martin CD, Kaiser PK, McCreath DR (1999) Hoek-brown parameters for predicting the depth of brittle failure around tunnels. Can Geotech J 36:136–151. https://doi.org/10.1139/t98-072
Mitri HS, Hughes R, Zhang Y (2011) New rock stress factor for the stability graph method. Int J Rock Mech Min Sci 48:141–145. https://doi.org/10.1016/j.ijrmms.2010.09.015

Nguyen TT, Do NA, Karasev MA, Kien DV, Dias D (2021) Influence of tunnel shape on tunnel lining behaviour. Proc Inst Civ Eng Geotech Eng 174:355–371. https://doi.org/10.1680/jgeen.20.00057

Olufe OJ (2021) Study of production drifts stability and assessment of reinforcement requirements at LKAB Konsuln test-mine levels 436 and 486 using geologic structures data, and modelling software–dips and unwedge: a part of dp1 project (mine layout and technology) of the sustainable underground mining (Sum) project. in.

Panji M, Koohsari H, Adampira M, Alielahi H, Marnani AJ (2016) Stability analysis of shallow tunnels subjected to eccentric loads by a boundary element method. J Rock Mech Geotech Eng 8:480–488. https://doi.org/10.1016/j.jrmge.2016.01.006

Potts DM (1999) Finite element analysis in geotechnical engineering. Thomas Telford, London, UK.

Qiu HZ, Chen XQ, Wu QH, Wang RC, Zhao WY, Qian KJ (2020) Deformation mechanism and collapse treatment of the rock surrounding a shallow tunnel based on on-site monitoring. J Mt Sci 17:2897–2914. https://doi.org/10.1007/s11629-020-6026-2

Rahmani F, Hosseini SM, Khezri A, Maleki M (2022) Effect of grid-form deep soil mixing on the liquefaction-induced foundation settlement, using numerical approach. Arab J Geosci 15(12):1112. https://doi.org/10.1007/s12517-022-10340-x

Rasouli MM, Mahyar M, Meshkabadi K (2011) Design of overall slope angle and analysis of rock slope stability of Chadormalu mine using empirical and numerical methods. Engineering 3:965–971. https://doi.org/10.4236/eng.2011.39119

Sainoki A, Mitri HS (2014) Dynamic behaviour of mining-induced fault slip. Int J Rock Mech Min Sci 66:19–29. https://doi.org/10.1016/j.ijrmms.2013.12.003

Sanei M, Faramarzi L, Goli S, Fahimifar A, Rahmati A, Mehinrad A (2015) Development of a new equation for joint roughness coefficient (JRC) with fractal dimension: a case study of Bakhtiary dam site in Iran. Arab J Geosci 8:465–475. https://doi.org/10.1007/s12517-013-1147-3

Selvasekaran R, Appuhami KA, Kumarasiri SA, Fernandopulle SN, Lakmal HM, Dharmaratne PG. Effects of joint orientation in tunneling.

Sinha S, Chugh Y (2018) Validation of critical strain technique for assessing stability of coal mine intersections and its potential for development of roof control plans. J Rock Mech Geotech Eng 10:380–389. https://doi.org/10.1016/j.jrmge.2017.10.003

Soren K, Budi G, Sen P (2014) Stability analysis of open pit slope by finite difference method. Int J Res Eng Technol 3(5):326–334

Tonon F, Amadei B (2003) Stresses in anisotropic rock masses: an engineering perspective building on geological knowledge. Int J Rock Mech Min Sci 40(7–8):1099–1120. https://doi.org/10.1016/j.ijrmms.2003.07.009

Wang T, Huang T (2009) A constitutive model for the deformation of a rock mass containing sets of ubiquitous joints. Int J Rock Mech Min Sci 46:521–530. https://doi.org/10.1016/j.ijrmms.2008.09.011

Wang C, Li G, Gao A, Shi F, Lu Z, Lu H (2018) Optimal preconditioning and support designs of floor heave in deep roadways. Geomech Eng 14:429–437. https://doi.org/10.12989/gae.2018.14.5.429

Wasantha PL, Habil HK (2015b) Geometrical properties of rock joints and their effects on rock mechanical behaviour. Internal Report.

Wang H, Li S, Wang Q, Wang D, Li W, Liu P, Li X, Chen Y (2019) Investigating the supporting effect of rock bolts in varying anchoring methods in a tunnel. Geomech Eng 19:485–498. https://doi.org/10.12989/gae.2019.19.6.485

Wasantha P, Guerrieri M, Xu T (2021) Effects of tunnel fires on the mechanical behaviour of rocks in the vicinity–a review. Tunn Undergr Sp Technol 108:103667. https://doi.org/10.1016/j.tust.2020.103667

Wu H, Ma D, Spearing A, Zhao G (2021) Fracture response and mechanisms of brittle rock with different numbers of openings under uniaxial loading. Geomech Eng 25:481–493. https://doi.org/10.12989/gae.2021.25.6.481

Yeung MR, Leong LL (1997) Effects of joint attributes on tunnel stability. Int J Rock Mech Min Sci 34(3–4):1–18. https://doi.org/10.1016/S1365-1609(97)00286-4

Yu ZH, Kulatilake PHSW, Jiang FX (2011) Effect of tunnel shape and support system on stability of a tunnel in a deep coal mine in China. In: proceedings of the 45th US rock mechanics/geomechanics symposium, San Francisco, USA, June 2011

Zaid M (2021) Dynamic stability analysis of rock tunnels subjected to impact loading with varying UCS. Geomech Eng 24:505–518. https://doi.org/10.12989/gae.2021.24.6.505

Zhang Y, Mitri HS (2008) Elastoplastic stability analysis of mine haulage drift in the vicinity of mined stopes. Int J Rock Mech Min Sci 45:574–593. https://doi.org/10.1016/j.ijrmms.2007.07.020

Zhang R, Yang X (2019) New 3D failure analysis of water-filled karst cave beneath deep tunnel. Geomech Eng 18:1–9. https://doi.org/10.12989/gae.2019.18.1.001

Zhang X, Zhang C, Min B, Xu Y (2020) Experimental study on the mechanical response and failure behavior of double-arch tunnels with cavities behind the liner. Geomech Eng 20:399–410. https://doi.org/10.12989/gae.2020.20.5.399

Zhou J, Yang XA (2021) Deformation behavior analysis of tunnels opened in various rock mass grades conditions in China. Geomech Eng 26:191–204. https://doi.org/10.12989/gae.2021.26.2.191

Zhou J, Chen Y, Li C, Qiu Y, Huang S, Tao M (2023) Machine learning models to predict the tunnel wall convergence. Transp Geotech 41:101022. https://doi.org/10.1016/j.trgeo.2023.101022